Calculation of Stress Intensity Factors in an Isotropic Multicracked Plate: Part II- Symbolic/Numeric Implementation

S. M. Arnold
National Aeronautics and Space Administration
Lewis Research Center
Cleveland, OH 44135

W. K. Binienda
University of Akron
Department of Civil Engineering
Akron, OH 44325

H. Q. Tan and M. H. Xu
University of Akron
Department of Mathematical Sciences
Akron, OH 44325

Abstract

Analytical derivations of stress intensity factors (SIF's) for a multicracked plate can be complex and tedious. Recent advances, however, in intelligent application of symbolic computation can overcome these difficulties and provide the means to rigorously and efficiently analyze this class of problems. Here, the symbolic algorithm required to implement the methodology described in Part I is presented. The special problem-oriented symbolic functions to derive the fundamental kernels are described, and the associated automatically generated FORTRAN subroutines are given. As a result, a symbolic/FORTRAN package named SYMFRAC, capable of providing accurate SIF's at each crack tip, has been developed and validated.

Simple illustrative examples using SYMFRAC show the potential of the present approach for predicting the macrocrack propagation path due to existing microcracks in the vicinity of a macrocrack tip, when the influence of the microcracks' location, orientation, size, and interaction are accounted for.

Nomenclature

β_{lr}, β_{mz}	–	direction cosines between two local coordinate systems
ϵ_{jl}	–	strain tensor
λ	–	offset of notch-microcracks system with respect to Y axis
μ_k	–	four roots of the characteristic equation
ν	–	Poisson's ratio
$\sigma^o_{jl}, \sigma^T_{jl}$	–	far-field and total stress field, respectively
$\sigma^o_{XX}, \sigma^o_{YY}, \sigma^o_{XY}$	–	components of stress in global coordinate system
φ_j	–	angle defining orientation of local coordinate system
ξ, τ	–	normalized real variables
$\Phi(s, y)$	–	Fourier transform of Airy stress function with respect to x variable

a_j	–	half crack length
a_{11}, a_{12}, a_{22}	–	coefficients of strain-stress relationship (compliant matrix)
d	–	normalized radial (tip) distance
$f_{\eta j}$	–	auxiliary functions
k_1, k_2	–	mode-I and mode-II stress intensity factors
$ker_{\gamma\delta}^{\alpha\beta}$	–	Fredholm kernels
p_j	–	normal traction at crack surface
q_j	–	shear traction at crack surface
s	–	Fourier variable
$\underline{r_j}$	–	position vector defining the origin of a local coordinate system
r_{jX}, r_{jY}	–	components of the position vector $\underline{r_j}$
u, v	–	displacement associated with the x and y coordinates, respectively
w	–	weight function
x_j, y_j and X, Y	–	local and global coordinates
$[A]$	–	kernel matrix
C_j', C_j	–	functions of s in Fourier space (i.e., constants in x, y-real space)
E	–	Young's modulus
$F_j(x_j, y_j)$	–	Airy stress function
$G_{\eta j}(\tau_p)$	–	discrete auxiliary function
$\{\mathcal{R}\}$	–	loading vector

1 Introduction

The computer has become an indispensable tool for both engineering analysis and design. Advanced computing techniques provide powerful tools for computationally-intense applications in engineering. Symbolic computation specializes in the exact computation with numbers, formulas, vectors, matrices, equations, and the like. Numerical computation, on the other hand, uses floating-point numbers, and approximates computations to solve problems of practical interest. The two approaches are complementary and, when combined into an integrated form, can be very powerful for engineering applications.

Analyzing the interaction of microcracks analytically, as discussed in Part I (Binienda et al. 1992), involves extensive manipulation of complex mathematical expressions. To date, the methodology has been developed for analyzing multiple cracks within an isotropic material. A similar methodology can be implemented for anisotropic and/or nonhomogeneous materials, and for complex, nonstraight multicracked configurations. However, because of the complexities involved, it is impossible for researchers to investigate this general problem without relying on the power of symbolic computations.

Presented here is a symbolic manipulation package (SYMFRAC, from SYMbolic FRACture) capable of providing both analytic derivation and FORTRAN code generation for n straight, fully interacting cracks in an isotropic plate that is subjected to in-plane loading. The immediate benefits that can be realized are (1) reduced tedium of manual derivation, (2) increased reliability of the derived equations and, hence, the final analysis results, and (3) improved numerical efficiency and accuracy for multiple interacting cracks.

This paper begins with a description of the associated symbolic algorithm and is followed by subsequent sections describing in detail the three key steps involved in the underlying formulation given in Part I (Binienda et al. 1992). It concludes with two numerical examples that illustrate the major capabilities of SYMFRAC: (1) a four-crack problem in which three microcracks interact

with a larger notch and (2) a fully interacting multicrack problem, with two notches and eight microcracks.

2 Computational Algorithm

The general theoretical formulation for a multicrack mixed boundary value problem has been discussed in Part I (Binienda et al. 1992) and can be classified into four main steps: (1) the derivation of the local stress equations for each crack in its respective local coordinate system, (2) formulation of the total perturbation stress field for each crack, (3) formulation of the singular integral system of equations, and (4) the solution for the stress intensity factors of this singular integral system via the discrete auxiliary functions.

Each of these basic steps involve numerous, tedious intermediate steps; this suggests that symbolic computations may be an attractive tool for automating the derivation and solution of this class of mixed boundary value problems.

The required algorithm to accomplish such automation can be divided into the following 11 steps.

(1) Convert the governing equation,

$$\frac{\partial^4}{\partial x^4}F(x,y) + \frac{2\partial^4}{\partial x^2 \partial y^2}F(x,y) + \frac{\partial^4}{\partial y^4}F(x,y) = 0 \tag{1}$$

into an ODE by Fourier transform; that is,

$$s^4\Phi - s^2\Phi'' + \Phi'''' = 0 \tag{2}$$

(2) Solve the ODE. For the isotropic case, the roots of the characteristic equation are two identical real roots; thus the general solution is

$$(C_1' + C_2'y)e^{ys} + (C_3' + C_4'y)e^{-ys} \tag{3}$$

(3) Use the inverse Fourier transformation and the condition that $F(x,y)$ must go to zero at infinity, to obtain the following Airy's stress function:

$$F(x,y^+) = \frac{1}{2\pi}[(C_1 + C_2y)e^{-|s|y}e^{-isx}] \qquad for \;\; y > 0 \tag{4}$$

and

$$F(x,y^-) = \frac{1}{2\pi}[(C_3 + C_4y)e^{|s|y}e^{-isx}] \qquad for \;\; y < 0 \tag{5}$$

where $C_j (j = 1, ..., 4)$ are arbitrary functions of s.

(4) Find the stress, strains, and displacements through differentiating, applying a constitutive relationship and integrating with respect to strain.

(5) Introduce auxiliary functions $f_1(x)$ and $f_2(x)$ such that

$$f_1(x) = \frac{\partial}{\partial x}[u^+(x,0) - u^-(x,0)]. \tag{6}$$

and

$$f_2(x) = \frac{\partial}{\partial x}[v^+(x,0) - v^-(x,0)]. \tag{7}$$

(6) Solve for C_1, C_2, C_3, and C_4 in terms of the auxiliary functions $f_1(x)$ and $f_2(x)$ by using the continuity conditions for σ_{yy} and σ_{xy}; that is,

$$\sigma_{yy}^{+}(x,0) = \sigma_{yy}^{-}(x,0) \tag{8}$$

$$\sigma_{xy}^{+}(x,0) = \sigma_{xy}^{-}(x,0) \tag{9}$$

(7) Find the final form by substituting the local stresses in terms of the auxiliary functions $f_1(x)$ and $f_2(x)$, and integrate with respect to the Fourier variable.

(8) Find the total stresses

$$_j\sigma_{rz}^{T}(x_j, y_j) = \sigma_{rz}^{j}(x_j, y_j) + \sum_{p=1}^{n-1} \sigma_{rz}^{'p}[x_p(x_j, y_j), y_p(x_j, y_j)] \tag{10}$$

by using coordinate transformations,

$$r_{jX} + x_j \cos\varphi_j - y_j \sin\varphi_j = r_{pX} + x_p \cos\varphi_p - y_p \sin\varphi_p \tag{11}$$

$$r_{jY} + x_j \sin\varphi_j + y_j \cos\varphi_j = r_{pY} + x_p \sin\varphi_p + y_p \cos\varphi_p \tag{12}$$

and the stress transformations

$$\sigma_{rz}^{'} = \beta_{lr}\beta_{mz}\sigma_{lm} \tag{13}$$

where β_{lr}, β_{mz} are the direction cosines for the (x_k, y_k) and (x_p, y_p) coordinate systems.

(9) Identify the Fredholm kernels ($\ker_p$) and normalize them, where $p = 1, 2, 3, 4$.

(10) Apply a collocation technique and generate the FORTRAN subroutine for the discrete auxiliary function vector {G}:

$$\{G\} = [A]^{-1}\{\mathcal{R}\} \tag{14}$$

where [A] is a fully populated matrix of the coefficients obtained from the Fredholm kernels, and $\{\mathcal{R}\}$ is the applied loading function.

(11) Evaluate the stress intensity factors (SIF's).

2.1 Symbolic Algorithm for Local Stress Formulation

The general form of the Airy stress function $F(x, y)$ for a plane problem is given in terms of the four unknown coefficients C_1 to C_4 (see Eqs. (4) and (5)). Two of the four are dependent because of the continuity conditions. The remaining two may be expressed conveniently in terms of the auxiliary functions as shown in Part I (Binienda et al. 1992). Substituting C_1 to C_4, as described in Part I into the stress equation for $y > 0$ or $y < 0$, the stress equations become

$$\sigma_{xx} = \int_{-a}^{a}\int_{-\infty}^{\infty}\{s^2[\frac{if_2(t)ye^{ist}}{4a_{11}s} - \frac{f_1(t)ye^{ist}}{4a_{11}|s|} + \frac{if_2(t)e^{ist}}{4a_{11}s|s|}]e^{-|s|y-isx}$$
$$- 2|s|[\frac{if_2(t)e^{ist}}{4a_{11}s} - \frac{f_1(t)e^{ist}}{4a_{11}|s|}]e^{-|s|y-isx}\}dsdt \tag{15}$$

$$\sigma_{yy} = \int_{-a}^{a}\int_{-\infty}^{\infty}\{-s^2[\frac{if_2(t)ye^{ist}}{4a_{11}s} - \frac{f_1(t)ye^{ist}}{4a_{11}|s|} + \frac{if_2(t)e^{ist}}{4a_{11}s|s|}]e^{-|s|y-isx}\}dsdt \tag{16}$$

$$\sigma_{xy} = \int_{-a}^{a}\int_{-\infty}^{\infty}\{is|s|[\frac{if_2(t)ye^{ist}}{4a_{11}s} - \frac{f_1(t)ye^{ist}}{4a_{11}|s|} + \frac{if_2(t)e^{ist}}{4a_{11}s|s|}]e^{-|s|y-isx}$$

$$- is[\frac{if_2(t)e^{ist}}{4a_{11}s} - \frac{f_1(t)e^{ist}}{4a_{11}|s|}]e^{-|s|y-isx}\}dsdt \tag{17}$$

In Eqs. (15) to (17) the range of integration is $-a \leq t \leq a$ for the coordinate variable and $-\infty < s < \infty$ for the Fourier variable. Integration with respect to the Fourier variable s can be separated into a negative portion $(-\infty, 0]$ and a positive portion $[0, +\infty)$. Then the variable of integration can be substituted, with $s' = -s$, and the order of integration switched such that all integration is over the domain $[0, +\infty)$. Hence, the stress equations are

$$\sigma_{xx} = \int_{-a}^{a}\int_{0}^{\infty}\{-\frac{isf_2(t)ye^{-sy+isx-ist}}{4a_{11}} - \frac{sf_1(t)ye^{-sy+isx-ist}}{4a_{11}}$$

$$+\frac{if_2(t)e^{-sy+isx-ist}}{4a_{11}} + \frac{f_1(t)e^{-sy+isx-ist}}{2a_{11}}$$

$$+\frac{isf_2(t)ye^{-sy-isx+ist}}{4a_{11}} - \frac{sf_1(t)ye^{-sy-isx+ist}}{4a_{11}}$$

$$-\frac{if_2(t)e^{-sy-isx+ist}}{4a_{11}} + \frac{f_1(t)e^{-sy-isx+ist}}{2a_{11}}\}dsdt \tag{18}$$

$$\sigma_{yy} = \int_{-a}^{a}\int_{0}^{\infty}\{\frac{isf_2(t)ye^{-sy+isx-ist}}{4a_{11}} + \frac{sf_1(t)ye^{-sy+isx-ist}}{4a_{11}}$$

$$+\frac{if_2(t)e^{-sy+isx-ist}}{4a_{11}} - \frac{isf_2(t)ye^{-sy-isx+ist}}{4a_{11}}$$

$$+\frac{sf_1(t)ye^{-sy-isx+ist}}{4a_{11}} - \frac{if_2(t)e^{-sy-isx+ist}}{4a_{11}}\}dsdt \tag{19}$$

$$\sigma_{xy} = \int_{-a}^{a}\int_{0}^{\infty}\{-\frac{isf_2(t)ye^{-sy+isx-ist}}{4a_{11}} + \frac{isf_1(t)ye^{-sy+isx-ist}}{4a_{11}}$$

$$-\frac{if_1(t)e^{-sy+isx-ist}}{2a_{11}} - \frac{sf_2(t)ye^{-sy-isx+ist}}{4a_{11}}$$

$$-\frac{isf_1(t)ye^{-sy-isx+ist}}{4a_{11}} + \frac{if_1(t)e^{-sy-isx+ist}}{2a_{11}}\}dsdt \tag{20}$$

It is important to note that at this stage the function **integrate** in MACSYMA (MATHLAB GROUP 1984) cannot be applied directly to perform the previous integration because of the occurrence of an infinite loop. Instead, intermediate variables are introduced into the integrals and

the following recursive forms are applied in a heuristic manner to actually perform the required integration; that is,

$$I_1 = \int_0^\infty e^{\rho s} ds \qquad where \;\; \rho = \rho(x, -y, t) \tag{21}$$

and

$$I_n = \frac{\partial}{\partial y} I_{n-1} \qquad for \;\; n = 2, 3, ... \tag{22}$$

such that the result of the preceding integration (see Gradshteyn and Ryzhik 1980) is,

$$I_n = \frac{(-1)^n}{\rho^n} \qquad for \;\; n = 1, 2, 3, ... \tag{23}$$

For the isotropic case of n=1 and 2:

$$I_1 = -\frac{1}{-y \pm (x-t)i} \tag{24}$$

$$I_2 = \frac{1}{(-y \pm (x-t)i)^2} \tag{25}$$

Therefore, the resulting stresses become

$$\begin{aligned}\sigma_{xx} = \frac{1}{4\pi a_{11}} \int_{-a}^{a} \{ & f_2(t)(t-x)[\frac{-2y^2}{[y^2+(t-x)^2]^2} + \frac{1}{y^2+(t-x)^2}] \\ & - y f_1(t)[\frac{y^2-(t-x)^2}{[y^2+(t-x)^2]^2} - \frac{2}{y^2+(t-x)^2}]\} dt\end{aligned} \tag{26}$$

$$\begin{aligned}\sigma_{yy} = \frac{1}{4\pi a_{11}} \int_{-a}^{a} \{ & f_2(t)(t-x)[\frac{2y^2}{[y^2+(t-x)^2]^2} + \frac{1}{y^2+(t-x)^2}] \\ & + y f_1(t) \frac{y^2-(t-x)^2}{[y^2+(t-x)^2]^2}\} dt\end{aligned} \tag{27}$$

$$\begin{aligned}\sigma_{xy} = \frac{-1}{4\pi a_{11}} \int_{-a}^{a} \{ & f_1(t)(t-x)[\frac{2y^2}{[y^2+(t-x)^2]^2} - \frac{1}{y^2+(t-x)^2}] \\ & - y f_2(t) \frac{y^2-(t-x)^2}{[y^2+(t-x)^2]^2}\} dt\end{aligned} \tag{28}$$

The above evaluation of the Fourier integral is accomplished by invoking a single function called ISTRESS, thus making the details of this section transparent to the user.

2.2 Symbolic Algorithm for Fredholm Kernels

As we showed in Part I (Binienda et al. 1992), prior to obtaining the Fredholm kernels, we must compute the total stresses due to all cracks within the plate (see step (8), Eqs. (10) to (13)). We accomplish this through both coordinate and stress transformations of all surrounding cracks to a chosen j^{th} crack as described by Eq. (10). This transformation and summation procedure is continued until the total stress state (i.e., $({}_j\sigma^T_{yy})$ and $({}_j\sigma^T_{xy})$) at each crack surface has been found. Given the total stresses, we obtain the final form of the normalized Fredholm kernels by performing a variable transformation, (i.e., x=aξ; t=aτ; for -1$\leq$ ξ and τ $\leq$1) and applying crack boundary conditions (i.e., $y = 0$).

Hence, for the case of n cracks the whole system of singular integral equations is

$$
\begin{aligned}
{}_n\sigma^T_{xy} &= \tfrac{1}{4a_{11}}\Big\{\textstyle\int_{-1}^{1}\ker{}_1 f_{11}d\tau + \int_{-1}^{1}\ker{}_2 f_{12}d\tau \\
&+\ldots + \textstyle\int_{-1}^{1}\ker{}_1 f_{(n-1)1}d\tau + \int_{-1}^{1}\ker{}_2 f_{(n-1)2}d\tau + \frac{1}{\pi}\int_{-1}^{1}\frac{f_{n1}}{\tau-\xi}d\tau\Big\}
\end{aligned}
\tag{29}
$$

$$
\begin{aligned}
{}_n\sigma^T_{yy} &= \tfrac{1}{4a_{11}}\Big\{\textstyle\int_{-1}^{1}\ker{}_3 f_{11}d\tau + \int_{-1}^{1}\ker{}_4 f_{12}d\tau \\
&+\ldots + \textstyle\int_{-1}^{1}\ker{}_3 f_{(n-1)1}d\tau + \int_{-1}^{1}\ker{}_4 f_{(n-1)2}d\tau + \frac{1}{\pi}\int_{-1}^{1}\frac{f_{n2}}{\tau-\xi}d\tau\Big\}
\end{aligned}
\tag{30}
$$

where the four distinct kernels (i.e., $\ker_p$ for p=1,2,3,4) are shown in the Appendix of Part I (Binienda et al. 1992). These four kernels can be translated into FORTRAN code directly through the use of a built-in command in MACSYMA. The resulting generated code is given in Appendix A at the end of this paper. Note that these kernel functions are already modified by the associated Lobatto-Chebyshev parameters discussed in the next section.

2.3 Solution of Discrete Auxiliary Functions via the Collocation Technique

The Lobatto–Chebyshev collocation integration technique is used to transform the preceding system of singular integral equations (represented by Eqs. (29) and (30)) into a system of algebraic equations. These equations combined with the single valued conditions, described in Part I (Binienda et al. 1992), result in the following 2nm system of algebraic equations:

$$
\begin{aligned}
&\sum_{r=1}^{m}\Big[\frac{w_r f_{11}(\tau_r)}{\pi(\tau_r-\xi_z)} + \ker{}_1 f_{21}(\tau_r)w_r + \ker{}_2 f_{22}(\tau_r)w_r \\
&\cdots + \ker{}_1 f_{n1}(\tau_r)w_r + \ker{}_2 f_{n2}(\tau_r)w_r\Big] = 4a_{11}({}_1\sigma^T_{xy}) \\
&\qquad for \quad z = 1,\ldots,m-1
\end{aligned}
\tag{31}
$$

$$
\begin{aligned}
&\sum_{r=1}^{m}\Big[\frac{w_r f_{12}(\tau_r)}{\pi(\tau_r-\xi_z)} + \ker{}_3 f_{21}(\tau_r)w_r + \ker{}_4 f_{22}(\tau_r)w_r \\
&\cdots + \ker{}_3 f_{n1}(\tau_r)w_r + \ker{}_4 f_{n2}(\tau_r)w_r\Big] = 4a_{11}({}_1\sigma^T_{yy}) \\
&\qquad for \quad z = 1,\ldots,m-1
\end{aligned}
\tag{32}
$$

$$
\begin{aligned}
&\sum_{r=1}^{m}\Big[\ker{}_1 f_{21}(\tau_r)w_r + \ker{}_2 f_{22}(\tau_r)w_r + \frac{w_r f_{21}(\tau_r)}{\pi(\tau_r-\xi_z)} \\
&\cdots + \ker{}_1 f_{n1}(\tau_r)w_r + \ker{}_2 f_{n2}(\tau_r)w_r\Big] = 4a_{11}({}_2\sigma^T_{xy})
\end{aligned}
$$

$$for \quad z = 1, ..., m-1 \tag{33}$$

$$\sum_{r=1}^{m}[\ker_3 f_{21}(\tau_r)w_r + \ker_4 f_{22}(\tau_r)w_r + \frac{w_r f_{22}(\tau_r)}{\pi(\tau_r - \xi_z)}$$
$$\cdots + \ker_3 f_{n1}(\tau_r)w_r + \ker_4 f_{n2}(\tau_r)w_r] = 4a_{11}({}_2\sigma_{yy}^T)$$
$$for \quad z = 1, ..., m-1 \tag{34}$$

$$\vdots$$

$$\sum_{r=1}^{m}[\ker_1 f_{11}(\tau_r)w_r + \ker_2 f_{12}(\tau_r)w_r + \ker_1 f_{21}(\tau_r)w_r$$
$$+ \ker_2 f_{22}(\tau_r)w_r + \cdots + \frac{w_r f_{n1}(\tau_r)}{\pi(\tau_r - \xi_z)}] = 4a_{11}({}_n\sigma_{xy}^T)$$
$$for \quad z = 1, ..., m-1 \tag{35}$$

$$\sum_{r=1}^{m}[\ker_3 f_{11}(\tau_r)w_r + \ker_4 f_{22}(\tau_r)w_r + \ker_3 f_{21}(\tau_r)w_r$$
$$+ \ker_4 f_{22}(\tau_r)w_r + \cdots + \frac{w_r f_{n2}(\tau_r)}{\pi(\tau_r - \xi_z)}] = 4a_{11}({}_n\sigma_{yy}^T)$$
$$for \quad z = 1, ..., m-1 \tag{36}$$

$$\sum_{r=1}^{m} f_{11}(\tau_r)w_r = 0 \tag{37}$$

$$\sum_{r=1}^{m} f_{12}(\tau_r)w_r = 0 \tag{38}$$

$$\sum_{r=1}^{m} f_{21}(\tau_r)w_r = 0 \tag{39}$$

$$\sum_{p=1}^{m} f_{22}(\tau_p)w_p = 0 \tag{40}$$

$$\vdots$$

$$\sum_{r=1}^{m} f_{n1}(\tau_r)w_r = 0 \tag{41}$$

$$\sum_{r=1}^{m} f_{n2}(\tau_r)w_r = 0 \tag{42}$$

where m is the number of collocation points and τ_r, w_r and ξ_z are the associated abscissae, weights, and collocation points described in Part I (Binienda et al. 1992).

The above equations can be rewritten compactly by using matrix notation; that is,

$$[A]\{G\} = \{\mathcal{R}\} \tag{43}$$

where the kernel matrix [A] is shown in schematic form in Appendix B and the FORTRAN code to assemble this matrix is given in Appendix C. Similarly, the associated FORTRAN code to assemble the loading vector $\{\mathcal{R}\}$ is also shown in Appendix C.

Although, only two key FORTRAN subroutines have been shown here, an entire FORTRAN code named SYMFRAC has been developed. This code has the capability to calculate the stress intensity factors at each crack tip as defined in Part I (Binienda et al. 1992) for an isotropic plate subjected to an in-plane stress field with n cracks of arbitrary geometry. This code has been employed to give the numerical results in this paper and in Part I (Binienda et al. (1992)).

3 Numerical Application

In this section two problems of a cracked, brittle infinite isotropic plate are studied. The first problem is composed of a notch and three interacting microcracks. We will obtain mode-I and mode-II SIF's for the inner crack tips under two loading cases: normal and shear far field stress states. The geometry of this problem lacks any symmetry and represents a physical problem involving the influence of a cloud of microcracks on the fracture zone of a major notch. The second problem represents a symmetric crack configuration composed of two interacting sets of a notch and cloud of microcracks similar to problem 1. Here, however, each notch is associated geometrically with four interacting microcracks. This problem, which is also physically possible, illustrates various cases of propagation of two major notches that are influenced by their mutual interaction and, in addition, by the existence and interaction of a cloud of microcracks in front of these notches. Symmetry with respect to the origin of the global coordinate system is assumed in order to simplify the graphical reporting of SIF's obtained for all inner and some outer crack tips.

Macroscopically, the extension of the notch can be simulated through the connection with a surrounding microcrack. The specific microcrack involved, however, depends on the loading conditions and crack interaction effects (which are dependent upon the particular location, size and orientation of the surrounding microcracks). After identifying this specific microcrack we can assume that the microscopic extension of all cracks will occur in a self-similar manner. Consequently, the fastest growing microcrack will connect first with the notch, to create a large kinked or branched macrocrack (notch). The criterion for microcrack propagation is assumed to be represented by a critical SIF value. For the sake of illustration, let us also assume that the total critical SIF is a constant material property such that the maximum total SIF obtained by using mode-I and mode-II of the SIF's (k_1 and k_2) normalized with respect to the far field stress (σ^o_{jp}) and $\sqrt{a_1}$. Thus for the jth crack tip,

$$k^j_{total} = \sqrt{[(k^j_1)^2 + (k^j_2)^2]_{\max}} \tag{44}$$

is used as a crack selection criterion for propagation.

Clearly, alternative criteria for crack propagation can be selected; therefore to maximize the future utility of the present results, the SIF's are reported separately. Note, that the objective of these examples is not to examine the validity of a particular criterion, but merely to illustrate qualitatively the capabilities of SYMFRAC.

3.1 Interaction of One Notch With Three Microcracks

Consider the problem of the extension of a horizontal notch under two far field loading conditions; that is, a normal and a shear stress. Assume that within the fracture zone of the central notch, a cloud of microcracks has developed due to localized flaws, grain boundaries, *and/or* other fabrication and material factors. For the sake of simplicity, consider only three microcracks that are situated radially with respect to a horizontal notch, as shown in Fig. 1. The plate is subjected to the previously mentioned two loading conditions: Case 1 — a normal far field stress, and Case 2 — a shear far field stress.

3.1.1 Case 1: Normal stress, σ_{YY}

The variations of k_1 and k_2 for the inner crack tips as functions of the normalized distance d is shown in Figs. 2 and 3. The distances d_{12}, d_{13}, and d_{14} measured between the inner tips of the notch and microcracks 2, 3, and 4, respectively, are taken to be equal to each other (*i.e.*, $d = d_{12} = d_{13} = d_{14}$), and they are normalized with respect to half the notch length, a_1. The associated crack lengths, normalized with respect to a_1, are $a_1 = 1$ and $a_2 = a_3 = a_4 = 0.1$.

Figures 2 and 3 illustrate the mutual influence of the notch and microcracks on the mode-I and mode-II SIF's, respectively. Note that the significant influence of the notch on the SIF's of all microcracks begins once $d < 0.1$; however the notch continues to control (in that it will propagate in a self-similar manner), provided that the initial radial (tip) distance d of all microcracks is greater then 0.03. If $d < 0.03$, the mode-I SIF for crack 3 (oriented at 45°) becomes the largest, (see Fig. 2) Similarly, mode-II SIF for crack 3 dominates for all distances d, but in general it is much smaller than mode-I SIF's. The total SIF is the largest for crack 3 when d is approximately less then 0.075; therefore the 45° crack will grow to connect with the notch such that it will become a kinked macrocrack. It should also be noted that for this loading condition when d approaches infinity, mode-I SIF asymptotically becomes $\sqrt{a_j}\cos^2\theta$ and mode-II SIF becomes $\sqrt{a_j}sin\theta cos\theta$.

Now consider the influence of the size of inclined microcracks (*i.e.*, cracks 3 and 4). It can be observed from Figs. 4 and 5 that the length of microcrack 3 will accelerate self-similar crack propagation of the horizontal notch (due to a maximum k_1) until a_3 becomes larger than 0.95, whereupon k_{total} of crack 3 dominates. Thus, kinking will occur in the direction of crack 3. Alternatively, Figs. 6 and 7 show that self-similar extension of the notch is *independent* of the size of crack 4, the 90° crack. In fact, Fig. 6 shows that crack 4 shields the notch by reducing its SIF's once $a_4 > 0.8$.

Note, that in Figs. (4) to (7) the centers of the microcracks are maintained at $r_2 = r_3 = r_4 = 1$ (where $r_j = d_j + a_j$), while the length of the particular crack under consideration varies from 0 to 1 and the size of the other microcracks remain constant at $a_j = 0.1$.

3.1.2 Case 2: Shear stress, σ_{XY}

Next, a similar parametric study is conducted for the case when a far field shear stress is applied to the plate. As presented previously the variation of k_1 and k_2 with respect to d for the notch as well as all three microcracks is shown in Figs. 8 and 9, respectively. Clearly, the notch will grow in a self similar manner under mode-II for most values of d; however, the notch may kink in the direction of crack 3 if d is very small. The trend for mode-II, shown in Fig. 9, illustrates that for small values of d the SIF's of cracks 2 and 4 are reduced due to shielding effects. The dominant mode of fracture for the notch is mode II when $d > 0.03$.

Figures 10 and 11 show the mode-I and mode-II SIF's for the inner crack tips when the size of crack 3 is increased, while the centers of all other microcracks are held constant at $r_j = 1$. Results

indicate that for all lengths of crack 3, even those very large, the notch would not kink, but rather grow in a self-similar manner under mode-II conditions. Conversely, the SIF's calculated when the size of crack 4 (i.e., 90°) increased (see Figs. 12 and 13), indicate that the notch will grow (1) in a self-similar manner under mode-II conditions when $a_4 < 0.63$; (2) will kink in the direction of crack 4 when $0.63 < a_4 < 0.95$ under mixed-mode conditions; or (3) will propagate once again in a self-similar manner, but now predominantly under mode-I, when $a_4 > 0.95$.

3.2 Interaction of Two Notches With Eight Microcracks

Consider the problem of two horizontal microcracks, possessing sharp notches, embedded in a plate parallel to the X-axis (see Fig. 14). The plate is subjected to a normal stress σ_{YY} at infinity. Furthermore, assume that within the fracture zone of the notches, two clouds of microcracks have developed due to localized flaws, grain boundaries, and/or other fabrication and material factors. For the sake of simplicity, consider only four microcracks associated with each notch, such that they are situated radially with respect to each notch as shown in Fig. 14. The orientations of the microcracks within each cloud are 0°, 30°, 60°, and 90°, and the radial tip distance between the notch and its associated cloud of microcracks is d.

The second parameter characterizing the geometry of the multiple crack system is λ, which represents the offset of the system with respect to the global vertical axis Y. For the case of $\lambda > 0$, the lower system of cracks (i.e., notch 1 and microcracks 3,4,5, and 6) is shifted to the right of the vertical axis, whereas the upper system (notch 2 and cracks 7,8,9, and 10) is shifted to the left. Note: The origin of the global coordinate system X and Y is always taken to be the point of symmetry of the crack configuration. In this way the presentation of the results can be simplified; however, this in no way implies any restriction, due to the symmetry, on the calculation of the SIF's. Finally, the parameters d, λ, and the half crack lengths a_j ($j = 2, 3, 4, ..., 10$) are normalized with respect to the half notch length a_1 (where $a_1 = a_2$).

For convenience, the location of each crack's local coordinate system (i.e., center of the crack) is taken to depend upon the tip distance d, the offset λ, and the half crack length a_j. Hence, the centers of notches 1 and 2 are

$$r_{1X} = \lambda - a_1 \tag{45}$$

$$r_{1Y} = -(d + a_6) \tag{46}$$

and

$$r_{2X} = -r_{1X} \tag{47}$$

$$r_{2Y} = -r_{1Y} \tag{48}$$

and the centers of microcracks 3 through 6 and their counterpart microcracks (7 to 10) are

$$r_{jX} = \lambda + (d + a_j)\cos\varphi_j \tag{49}$$

$$r_{jY} = r_{1Y} + (d + a_j)\sin\varphi_j \tag{50}$$

$$r_{(13-j)X} = -r_{jX} \tag{51}$$

$$r_{(13-j)Y} = -r_{jY} \tag{52}$$

where r_{jX} and r_{jY} are the X and Y components, respectively, of the vector between the origin of the global and local coordinate systems and j =3,4,...,10.

3.2.1 Influence of crack tip distance d

Consider the case when $a_1 = a_2 = 1$, the offset λ is equal to 0.1, and the half length of each microcrack $a_j = 0.1$ (where $j = 3, 4, ..., 10$), and d varies from 0 to 0.5. The resulting inner SIF's k_1 and k_2 (representing mode I and mode II), are shown in Figs. 15 and 16, respectively. From examining the strength of k_1 and k_2, it is clear that for all d values mode I is dominant and for $d > 0.025$ the inner notch tip would propagate in a self-similar manner. However, for $d < 0.025$, the k_1 value for the 30° microcracks exceeds all other k_1 values, thus indicating propagation of the 30° microcracks and possible connection with the inner tip of the notch, thereby creating a macroscopic kinked crack. Although mode II (see Fig. 16) is significantly smaller in magnitude relative to mode I, and therefore does not play a role in the propagation of the various cracks, it is interesting to note that for $d > 0.025$ the 90° microcracks have a maximum k_2, whereas for $d < 0.025$ the 60° microcracks do. Also, as expected when d approaches 0.5 (i.e., 1/4 of the notch length) the influence of the microcracks on the k_1 of the notch is minimal. Clearly there are two competing mechanisms: the first reduces k_1 because of crack shielding (observed at high d values), and the other increases k_1 at small d values thereby simulating an increase in damage density at the notch tip that promotes crack propagation.

3.2.2 Influence of offset λ

Here, as in the previous case, $a_1 = a_2 = 1$ and $a_j = 0.1$ for $j = 3, 4, ...10$; but now d is held fixed at 0.1 while λ is varied from -0.5 to +0.5. As before, the inner SIF's (k_1 and k_2) are shown versus λ in Figs. 17 and 18. Note, that all cases in which microcrack overlap occurs (i.e., $-0.2 < \lambda < 0.15$) have been skipped. As in the previous section, two primary effects, one dealing with the "density" of the damage zone at the crack tip and the other with shielding are observed in Figs. 17 and 18. Clearly, in Fig. 17 as λ approaches -0.2 from the left, the "density" of the damage zone (characterized by the number of microcracks per unit length in front of the notches) increases, consequently increasing the strength of k_1. The second effect, again referring to k_1 in Fig.17, is attributed to the shielding for $\lambda > 0.15$ in that each notch shields the other as well as their associated cloud of microcracks. Again, although mode II values are smaller than those of mode I, it is interesting to note that k_2 of the notch becomes maximum when shielding occurs (i.e., $0.15 < \lambda < 0.5$).

3.2.3 Influence of microcrack lengths a_4 and a_5

Finally, the lengths of inclined cracks (e.g., 30° and 60°) are examined. Here, s is chosen to avoid crossing of the inclined crack with either notch. For example, consider the case in Figs. 19 and 20 where $a_1 = a_2 = 1.0$, $\lambda = 0.8$, $d = 0.1$, and $a_3 = a_5 = a_6 = 0.1$ while a_4 varies. Similarly, in Figs. 21 and 22 $a_1 = a_2 = 1.0$, $\lambda = 1.0$, $d = 0.1$, and $a_3 = a_4 = a_6 = 0.1$ as a_5 varies. In these figures (Figs. 19 to 22) in addition to all SIF's associated with the inner crack tips, the SIF's associated with the outer crack tips of the notches and the varying inclined microcracks are shown.

Comparison of Figs. 19 and 20 shows that mode I once again dominates. Therefore, let us focus our attention on the mode-I SIF for the outer tip of the notch. It is apparent that k_1=1 for values of $a_4 < 0.2$, thus indicating no crack interaction at this tip and propagation away from the damage zone. However, when $a_4 > 0.2$, k_1 for the outer crack tip dramatically drops off due to shielding by the 30° inclined microcrack associated with the opposite notch. Now focusing our attention on the k_1 associated with the inner tip of the 30° inclined microcrack, we see that for $a_4 > 0.2$ the present k_1 is maximum, thus indicating propagation of the inclined microcrack towards the associated notch; hence the potential kinking of the inner notch tip. Figure 19 illustrates the importance of the initial

damage configuration and its impact on the mechanism of crack propagation.

Comparing Figs. 21 and 22, which are associated with the case where the two notches are exactly aligned as shown in the inserts, we observe for the first time the potential dominance of mode-II SIF's. When $a_5 < 1.2$, both inner and outer notch tips are shielded because $k_1 < 1.0$. However, the inner notch tip SIF is higher than the outer tip SIF because of the interaction of the associated cloud of microcracks. Some additional shielding of the outer notch tip occurs when the length of the 60° microcrack is increased up to approximately 0.4.

4 Summary and Conclusion

The symbolic algorithm and key FORTRAN subroutines for constructing and calculating the SIF's, with the singular integral equation technique, for a multicracked mixed boundary value problem have been presented. This work has resulted in the development of special problem-oriented symbolic functions (e.g., ISTRESS) running under MACSYMA that simplify and automate the derivation process. Also MACSYMA's automatic FORTRAN generation capability has been utilized to produce the Fredholm kernel subroutines that constitute the core of the resulting FORTRAN portion of SYMFRAC.

The accuracy of the present technique was confirmed with available solutions in the literature for a two interacting crack problem shown in Part I. Also, two fully interacting multicrack problems were studied here to illustrate the capabilities of SYMFRAC.

Numerous observations where discussed using a simple crack propagation criterion. For example, (1) a notch-like crack can change its propagation direction (kink or branch) through connection with pre-existing microcracks; (2) the notch may propagate either toward or away from the surrounding cloud of microcracks; (3) two potential competing effects exist — shielding, which reduces the SIF's, and damage density, which increases the SIF's. In all of the preceding examples, results depend on the size, orientation, and distribution of the interacting cracks. Thus, the most important conclusion demonstrated is that the current damage configuration and the loading history dictate the future damage growth.

The power and usefulness of SYMFRAC is apparent in that the size, orientation and distribution of n fully interacting cracks in an isotropic plate can be studied. Furthermore, the methodology has now been established so that extension to more complex problems, in which anisotropic materials, kinked and branch cracks, and/or non-homogeneous materials are addressed, is straight-forward. Finally, it is apparent that the rigorous symbolic development of the system of singular integral equations and the associated automatic FORTRAN implementation is responsible for the speed and accuracy of the numerical calculations.

Appendix A - FORTRAN Code for the Discrete Fredholm Kernels

```
*****************************************************
*
* Calculate kr1 kr2 kr3 and kr4
*
*****************************************************
do 320 m=1,4
do 310 k=1,ncr
do 311 l=1,ncr
if (k .NE. l) then
r2x=rx(k)
r2y=ry(k)
gf2=gf(k)
a2=al(k)
r1x=rx(l)
r1y=ry(l)
gf1=gf(l)
a1=al(l)
gh=gf2-gf1
p1=(r2y-r1y)*dsin(gf1)+(r2x-r1x)*dcos(gf1)
p2=(r2y-r1y)*dcos(gf1)-(r2x-r1x)*dsin(gf1)
do 78 i=1,n-1
do 79 j=1,n
p1a1a2 = -p1+a1*gt(j)-a2*dcos(gh)*gc(i)
p2a2 = p2+a2*dsin(gh)*gc(i)
ww = p2a2**2+p1a1a2**2
wwm = p1a1a2**2-p2a2**2
if (m .EQ. 1) then
part1 = 2*dcos(2*gh)*p1a1a2*p2a2**2-dsin(2*gh)*p2a2*wwm
part1 = part1/ww**2
part2 = (-dsin(2*gh)*p2a2-dcos(2*gh)*p1a1a2)/ww
kr1((k-1)*n+i,(l-1)*n+j)=(a1/pi)*(part1+part2)*w(j)
else
if (m .EQ. 2) then
part1 = dcos(2*gh)*p2a2*wwm+2*dsin(2*gh)*p1a1a2*p2a2**2
part1 = part1/ww**2
kr2((k-1)*n+i,(l-1)*n+j)=(a1/pi)*part1*w(j)
else
if (m .EQ. 3) then
part1 = -dcos(2*gh)*p2a2*wwm-2*dsin(2*gh)*p1a1a2*p2a2**2
part1 = part1/ww**2
part2 = (2*dsin(gh)**2*p2a2+dsin(2*gh)*p1a1a2)/ww
kr3((k-1)*n+i,(l-1)*n+j)=(a1/pi)*(part1+part2)*w(j)
else
part1 = 2*dcos(2*gh)*p1a1a2*p2a2**2-dsin(2*gh)*p2a2*wwm
part1 = part1/ww**2
```

```
part2 = p1a1a2/ww
kr4((k-1)*n+i,(l-1)*n+j)=(a1/pi)*(part1+part2)*w(j)
end if
end if
end if
79 continue
78 continue
 end if
311 continue
310 continue
320 continue
**************************************************
```

Appendix B - Schematic Form of Kernel Matrix [A] and Load-Vector {R}

$$A = \begin{pmatrix} t & 0 & s^1_{12} & s^2_{12} & s^1_{13} & s^2_{13} & . & . & s^1_{1n} & s^2_{1n} \\ 0 & t & s^3_{12} & s^4_{12} & s^3_{13} & s^4_{13} & . & . & s^3_{1n} & s^4_{1n} \\ s^1_{21} & s^2_{21} & t & 0 & s^1_{23} & s^2_{23} & . & . & s^1_{2n} & s^2_{2n} \\ s^3_{21} & s^4_{21} & 0 & t & s^3_{23} & s^4_{23} & . & . & s^3_{2n} & s^4_{2n} \\ s^1_{31} & s^2_{31} & s^1_{32} & s^2_{32} & t & 0 & . & . & s^1_{3n} & s^2_{3n} \\ s^3_{31} & s^4_{31} & s^3_{32} & s^4_{32} & 0 & t & . & . & s^3_{3n} & s^4_{3n} \\ . & . & . & . & . & . & & & . & . \\ . & . & . & . & . & . & & & . & . \\ . & . & . & . & . & . & & & . & . \\ s^1_{n1} & s^2_{n1} & s^1_{n2} & s^2_{n2} & s^1_{n3} & s^2_{n3} & . & . & t & 0 \\ s^3_{n1} & s^4_{n1} & s^3_{n2} & s^4_{n2} & s^3_{n3} & s^4_{n3} & . & . & 0 & t \end{pmatrix}_{2nm*2nm}$$

where

$$t = \begin{pmatrix} \frac{w_1}{\pi(\tau_1-\xi_1)} & \cdots & \frac{w_m}{\pi(\tau_m-\xi_1)} \\ . & & . \\ . & & . \\ . & & . \\ \frac{w_1}{\pi(\tau_1-\xi_{m-1})} & \cdots & \frac{w_m}{\pi(\tau_m-\xi_{m-1})} \\ w_1 & \cdots & w_m \end{pmatrix}_{m*m}$$

$$s^i_{ab} = \begin{pmatrix} w_1 k_i(\tau_1, \xi_1, r_{x_a}, r_{x_b}, \ldots) & \ldots & w_m k_i(\tau_m, \xi_1, r_{x_a}, r_{x_b}, \ldots) \\ . & & . \\ . & & . \\ . & & . \\ w_1 k_i(\tau_1, \xi_{m-1}, r_{x_a}, r_{x_b}, \ldots) & \ldots & w_m k_i(\tau_m, \xi_{m-1}, r_{x_a}, r_{x_b}, \ldots) \\ 0 & \ldots & 0 \end{pmatrix}_{m*m}$$

where $i = 1, \ldots 4$; $a, b \in 1, \ldots n$; and $a \neq b$.

$$\{R\} = \begin{pmatrix} \tau^1 \\ \sigma^1 \\ \tau^2 \\ \sigma^2 \\ \cdot \\ \cdot \\ \cdot \\ \tau^n \\ \sigma^n \end{pmatrix}$$

where

$$\tau^i = \begin{pmatrix} \tau_{xy}^{iT} \\ \\ \tau_{xy}^{iT} \\ \cdot \\ \cdot \\ \cdot \\ \tau_{xy}^{iT} \end{pmatrix}$$

$$\sigma^i = \begin{pmatrix} \sigma_{yy}^{iT} \\ \\ \sigma_{yy}^{iT} \\ \cdot \\ \cdot \\ \cdot \\ \sigma_{yy}^{iT} \end{pmatrix}$$

Appendix C - FORTRAN Listing for Assemblage of Kernel Matrix [A] and Load Vector {R}

The FORTRAN code for matrix [A] is

```
**************************************************
*
* Calculate the diagonal elements of matrix [A]
*
**************************************************
 do 305 k=0,(2*ncr-1)
do 50 j=1,n
do 40 i=1,n-1
a(k*n+i,k*n+j)=w(j)/(pi*(gt(j)-gc(i)))
40 continue
 a((k+1)*n,k*n+j)=w(j)
50 continue
305 continue
**************************************************
*
* Combine kr1,kr2,kr3 and kr4 to calculate matrix [A]
* Input kr1 kr2 kr3 and kr4 to [A]
*
**************************************************
 do 350 k=0,ncr-1
do 351 l=0,ncr-1
if (k .NE. l) then
do 352 i=1,n-1
do 353 j=1,n
a(2*k*n+i,2*l*n+j)=kr1(k*n+i,l*n+j)
a(2*k*n+i,2*l*n+n+j)=kr2(k*n+i,l*n+j)
a(2*k*n+n+i,2*l*n+j)=kr3(k*n+i,l*n+j)
a(2*k*n+n+i,2*l*n+n+j)=kr4(k*n+i,l*n+j)
353 continue
352 continue
 end if
351 continue
350 continue
**************************************************
```

The FORTRAN code for matrix [R] is

```
*****************************************************
*
* Calculation of the right hand side of the systems equations R
*
*****************************************************
 do 370 i=1,ncr
gsyiyi(i)=gs0xx*dsin(gf(i))**2+gs0yy*dcos(gf(i))**2
gsyiyi(i)=gsyiyi(i)-gt0xy*dsin(2*gf(i))
gtxiyi(i)=-(gs0xx-gs0yy)/2*dsin(2*gf(i))+gt0xy*dcos(2*gf(i))
pixi(i)=-gsyiyi(i)
qixi(i)=-gtxiyi(i)
370 continue
 do 380 k=0,ncr-1
do 381 i=1,n-1
R(2*k*n+i)=-4*a11*qixi(k+1)
381 continue
380 continue
 do 382 k=0,ncr-1
do 383 i=1,n-1
R(2*k*n+n+i)=-4*a11*pixi(k+1)
383 continue
382 continue
*****************************************************
```

5 References

Binienda, W.K., Arnold S. M., Tan H. Q. (1992): Calculation of Stress Intensity Factors in an Isotropic Multi-cracked Plate: Part I - Theoretical Formulation. NASA TM 105766.

Gradshteyn, I.S., Ryzhik I.M. (1980): Tables of Integrals, Series and Products. Academic Press, New York.

MACSYMA (1984): MACSYMA Reference Manual. Version 10, The MATHLAB Group, Laboratory for Computer Science, MIT.

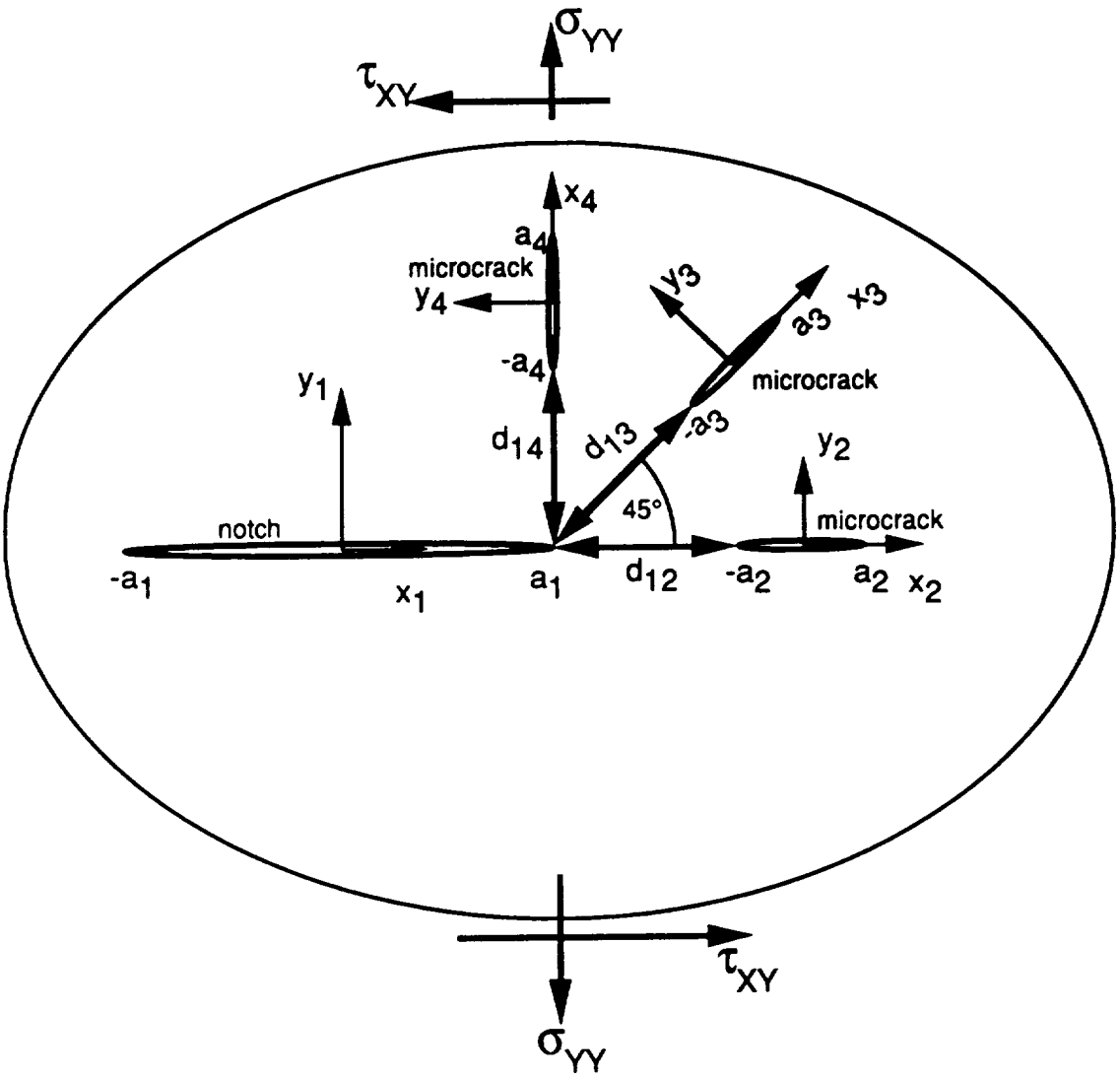

Fig. 1. Geometry describing the interaction one notch with three microcracks.

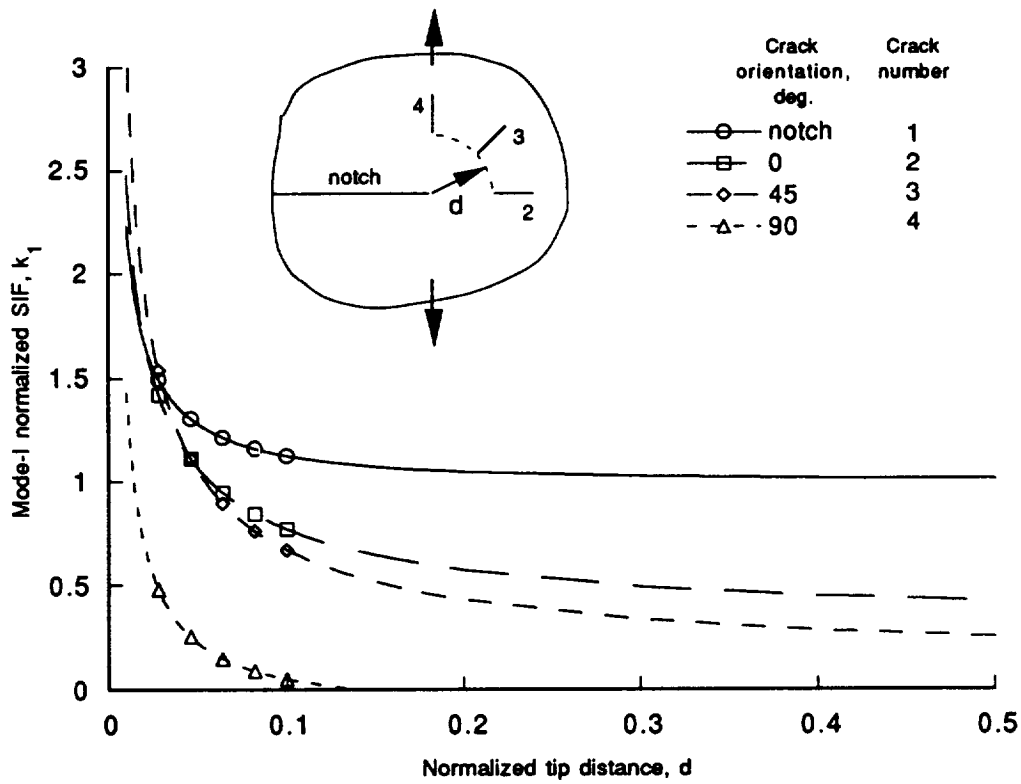

Fig. 2. Mode-I normalized SIF, k_1, for the inner crack tips versus the normalize tip distance d ($d = d_{12} = d_{13} = d_{14}$). Normal far field stress, σ_{YY}, load case.

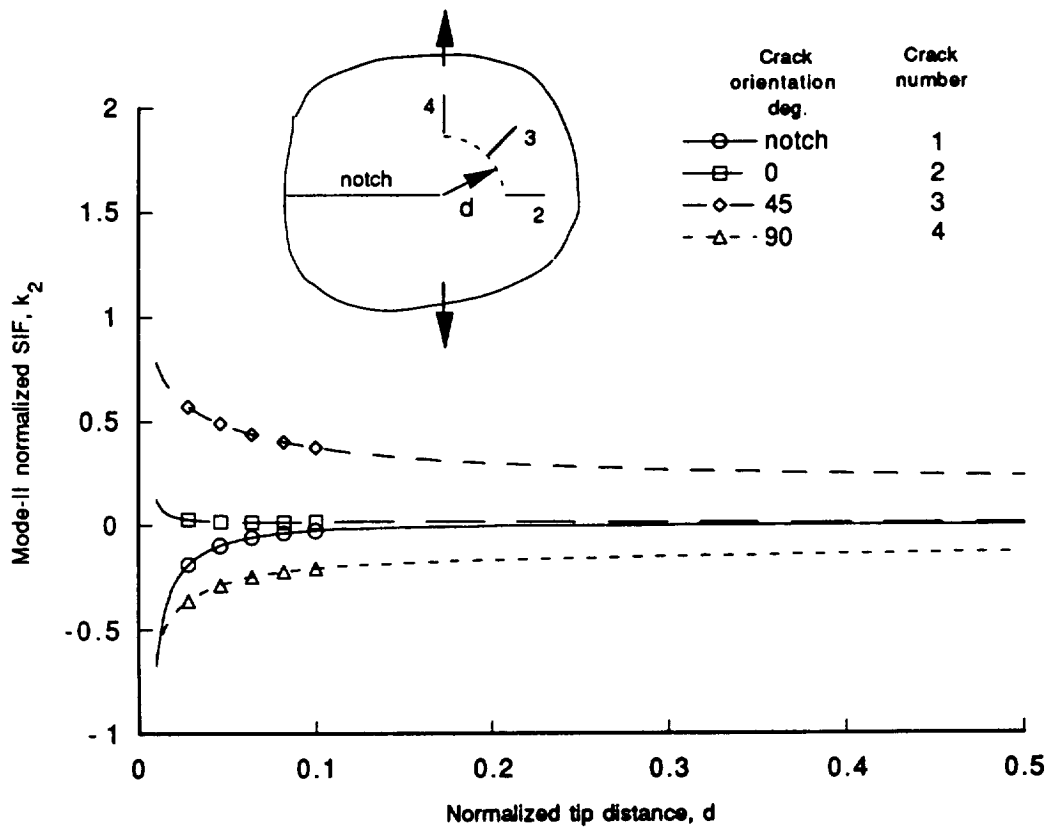

Fig. 3. Mode-II normalized SIF, k_2, for the inner crack tips versus the normalize tip distance d ($d = d_{12} = d_{13} = d_{14}$). Normal far field stress, σ_{YY}, load case.

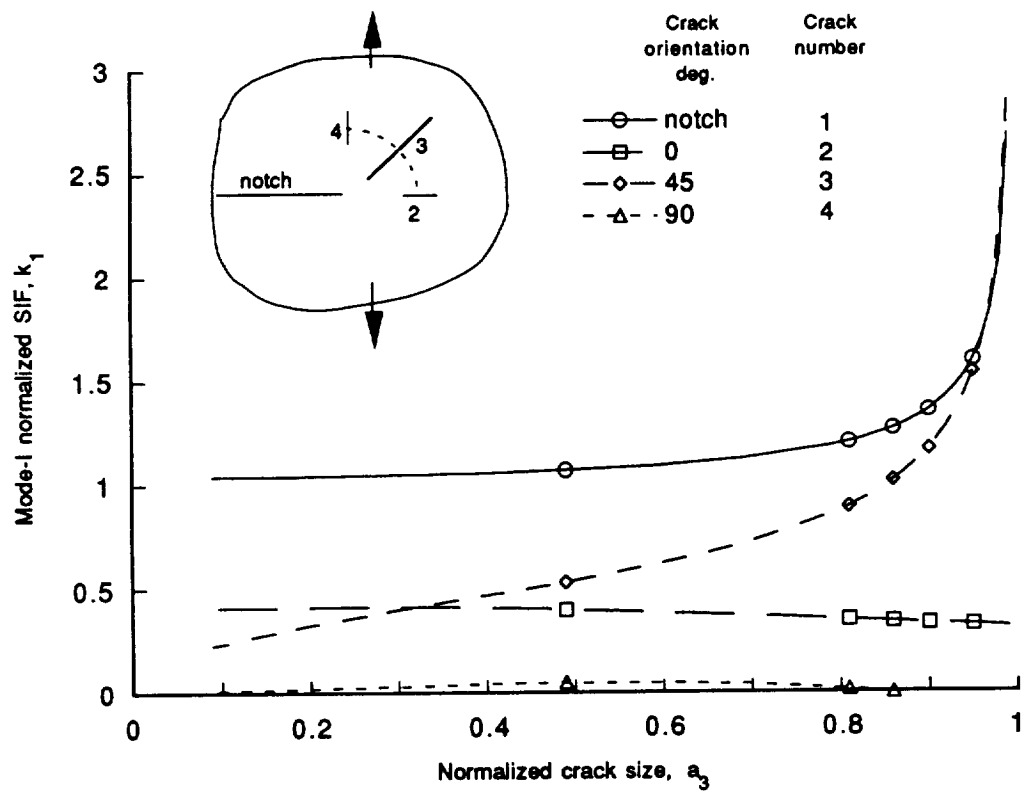

Fig. 4. Mode-I normalized SIF, k_1, for the inner crack tips versus the normalize crack size a_3 ($a_2 = a_4 = 0.1$, constant distance between the center of each crack to the origin of the global coordinate system, $|r_j| = 1$). Normal far field stress, σ_{YY}, load case.

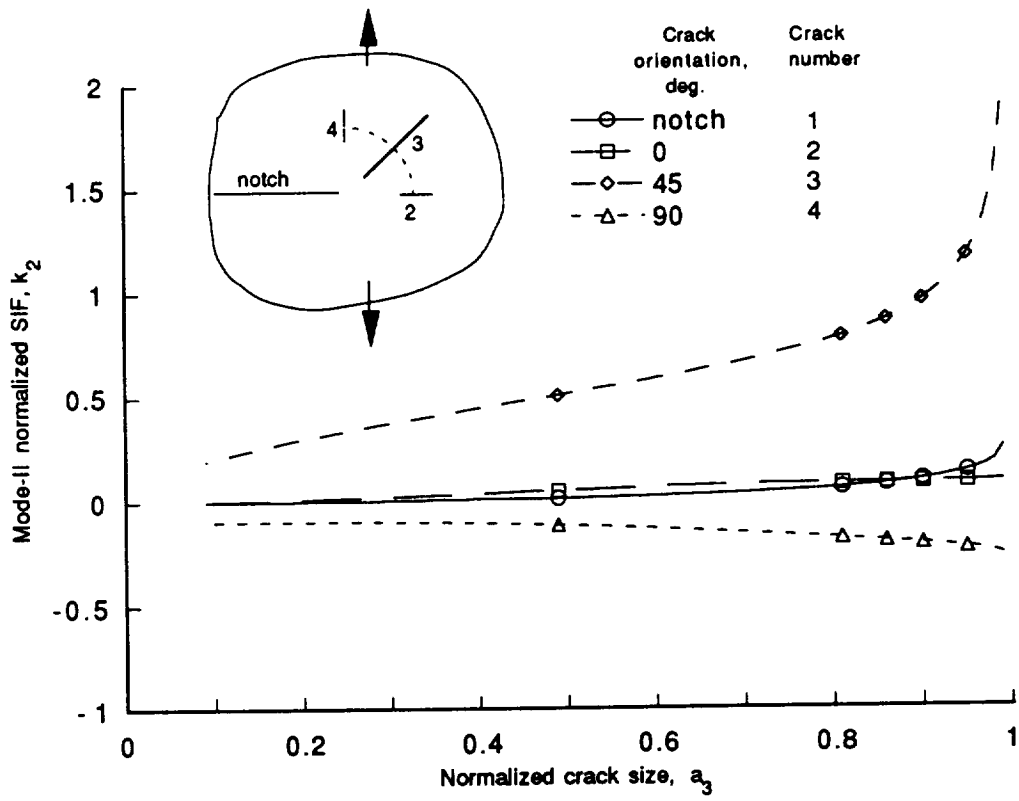

Fig. 5. Mode-II normalized SIF, k_2, for the inner crack tips versus the normalize crack size a_3 ($a_2 = a_4 = 0.1$, constant distance between the center of each crack to the origin of the global coordinate system, $|r_j| = 1$). Normal far field stress, σ_{YY}, load case.

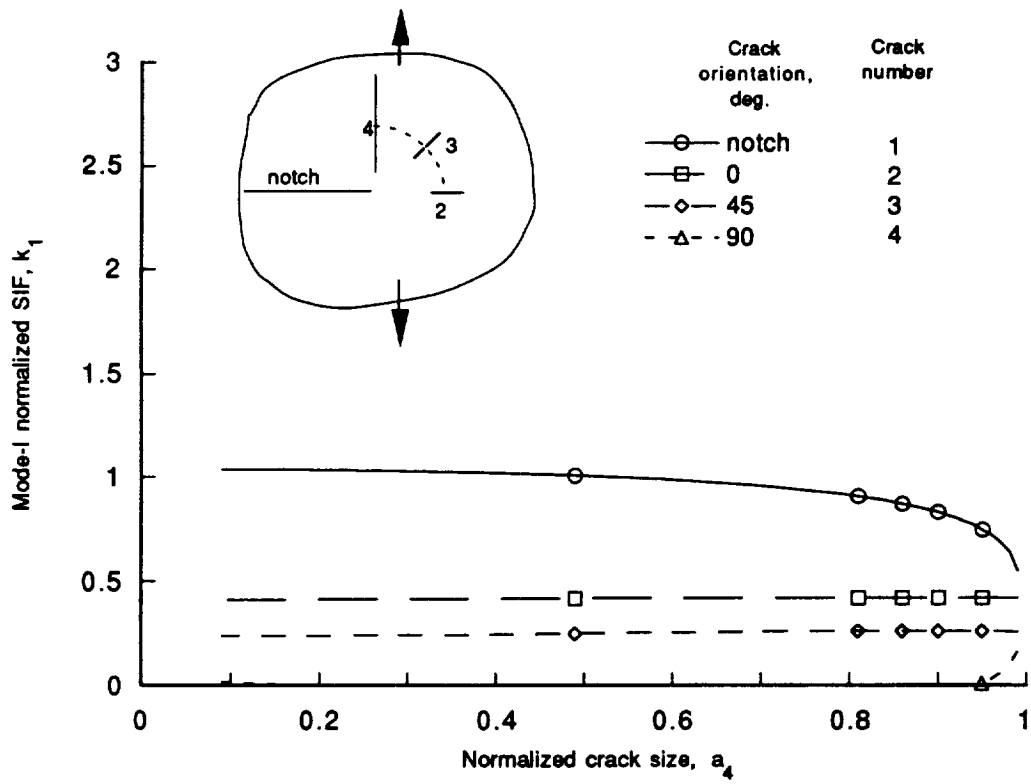

Fig. 6. Mode-I normalized SIF, k_1, for the inner crack tips versus the normalize crack size a_4 ($a_2 = a_3 = 0.1$, constant distance between the center of each crack to the origin of the global coordinate system, $|r_j| = 1$). Normal far field stress, σ_{YY}, load case.

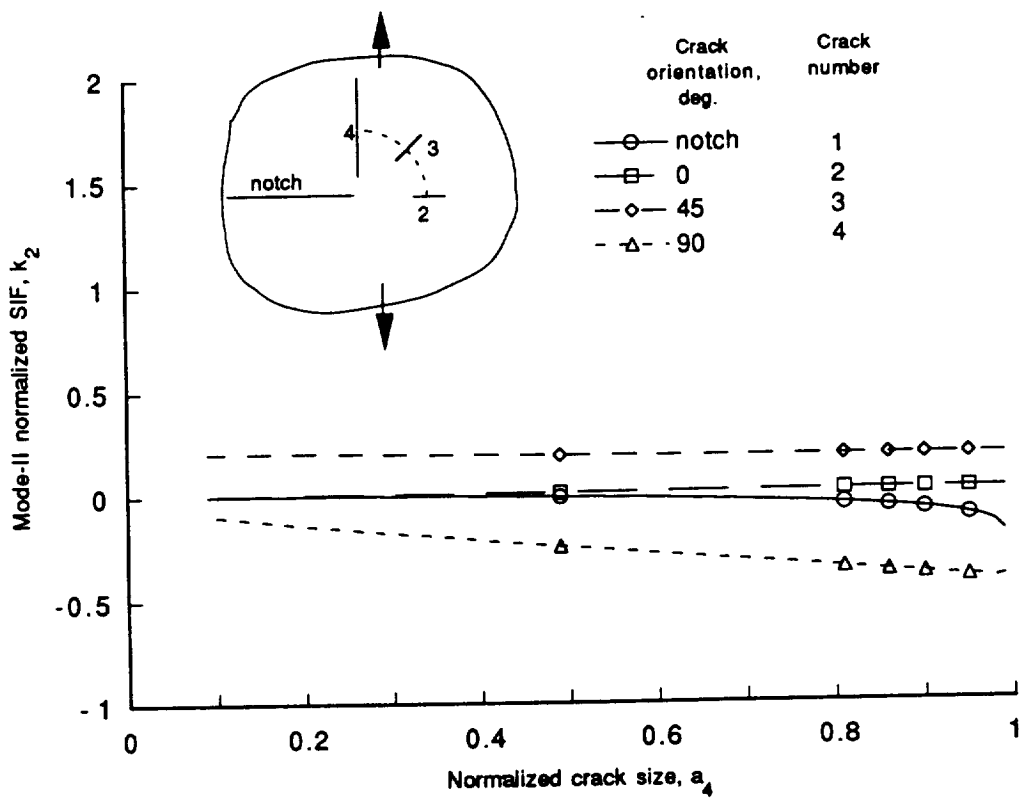

Fig. 7. Mode-II normalized SIF, k_2, for the inner crack tips versus the normalize crack size a_4 ($a_2 = a_3 = 0.1$, constant distance between the center of each crack to the origin of the global coordinate system, $|r_j| = 1$). Normal far field stress, σ_{YY}, load case.

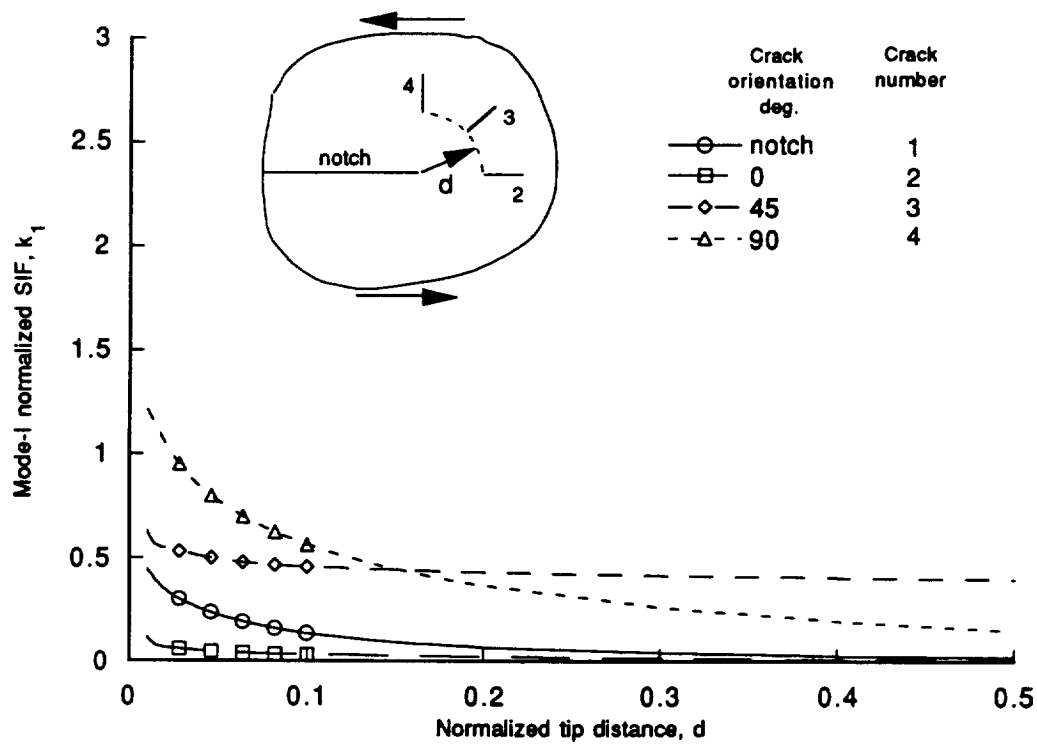

Fig. 8. Mode-I normalized SIF, k_1, for the inner crack tips versus the normalize tip distance d ($d = d_{12} = d_{13} = d_{14}$). Shear far field stress, σ_{XY}, load case.

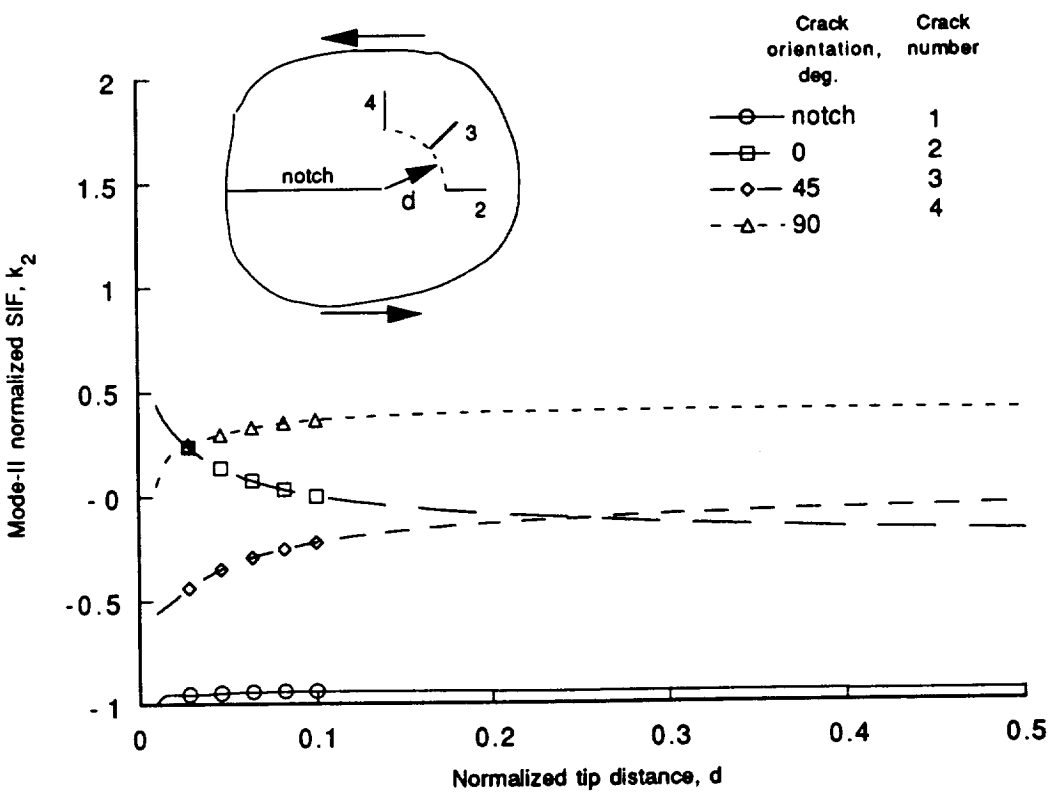

Fig. 9. Mode-II normalized SIF, k_2, for the inner crack tips versus the normalize tip distance d ($d = d_{12} = d_{13} = d_{14}$). Shear far field stress, σ_{XY}, load case.

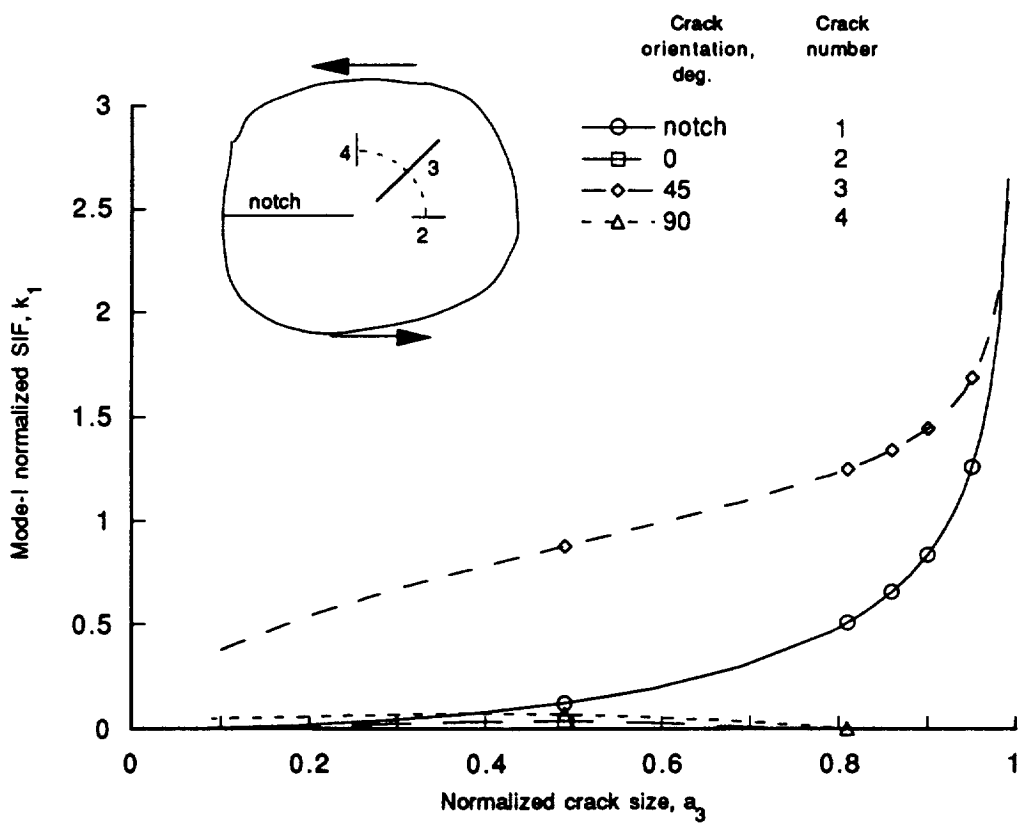

Fig. 10. Mode-I normalized SIF, k_1, for the inner crack tips versus the normalize crack size a_3 ($a_2 = a_4 = 0.1$, constant distance between the center of each crack to the origin of the global coordinate system, $|r_j| = 1$). Shear far field stress, σ_{XY}, load case.

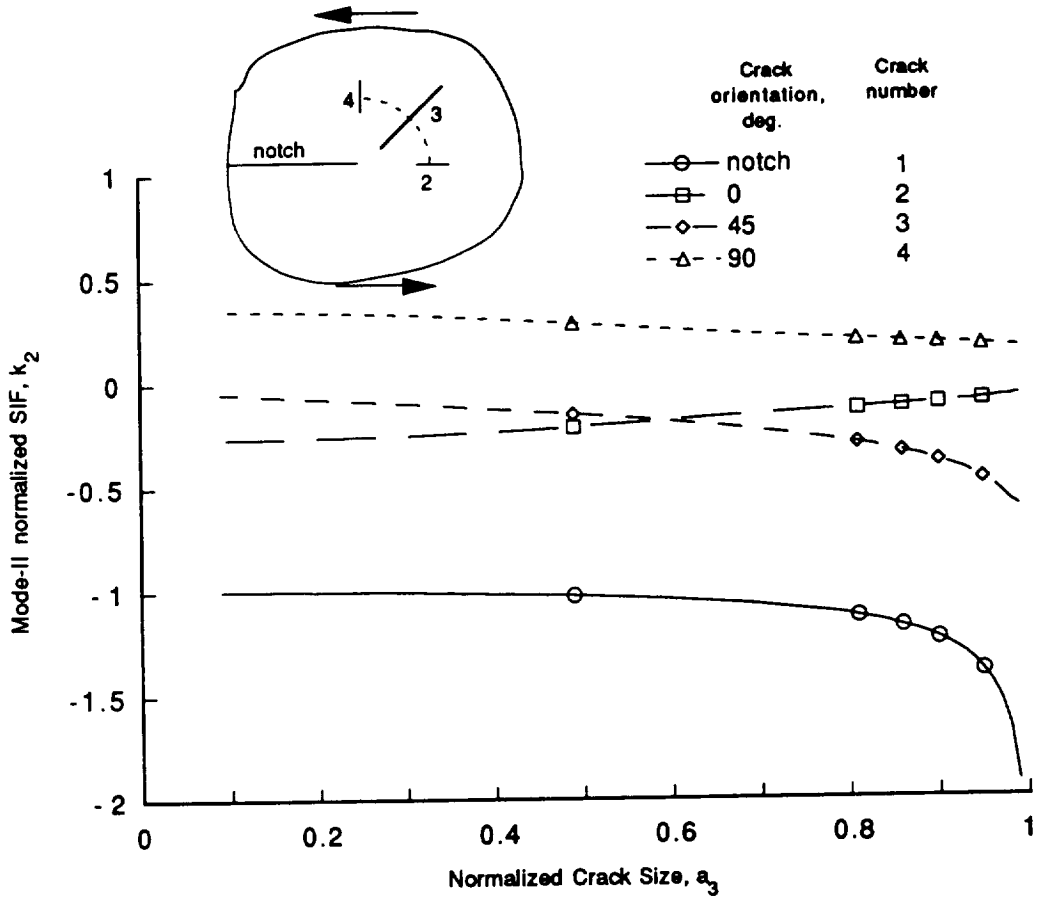

Fig. 11. Mode-II normalized SIF, k_2, for the inner crack tips versus the normalize crack size a_3 ($a_2 = a_4 = 0.1$, constant distance between the center of each crack to the origin of the global coordinate system, $|r_j| = 1$). Shear far field stress, σ_{XY}, load case.

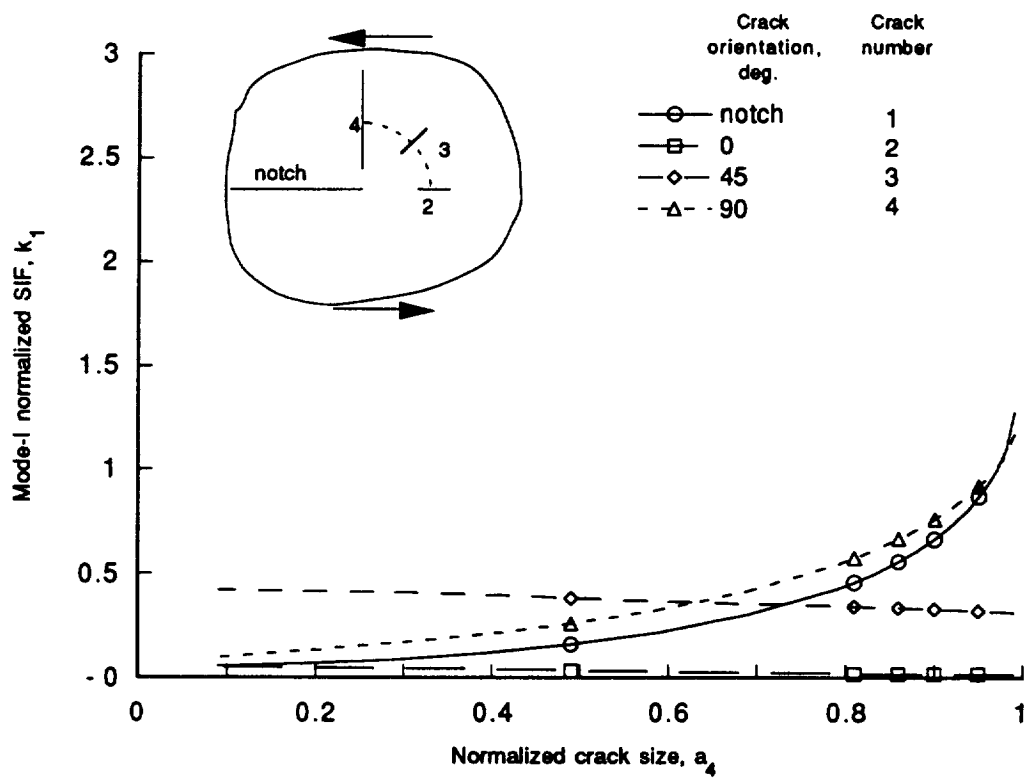

Fig. 12. Mode-I normalized SIF, k_1, for the inner crack tips versus the normalize crack size a_4 ($a_2 = a_3 = 0.1$, constant distance between the center of each crack to the origin of the global coordinate system, $|r_j| = 1$). Shear far field stress, σ_{XY}, load case.

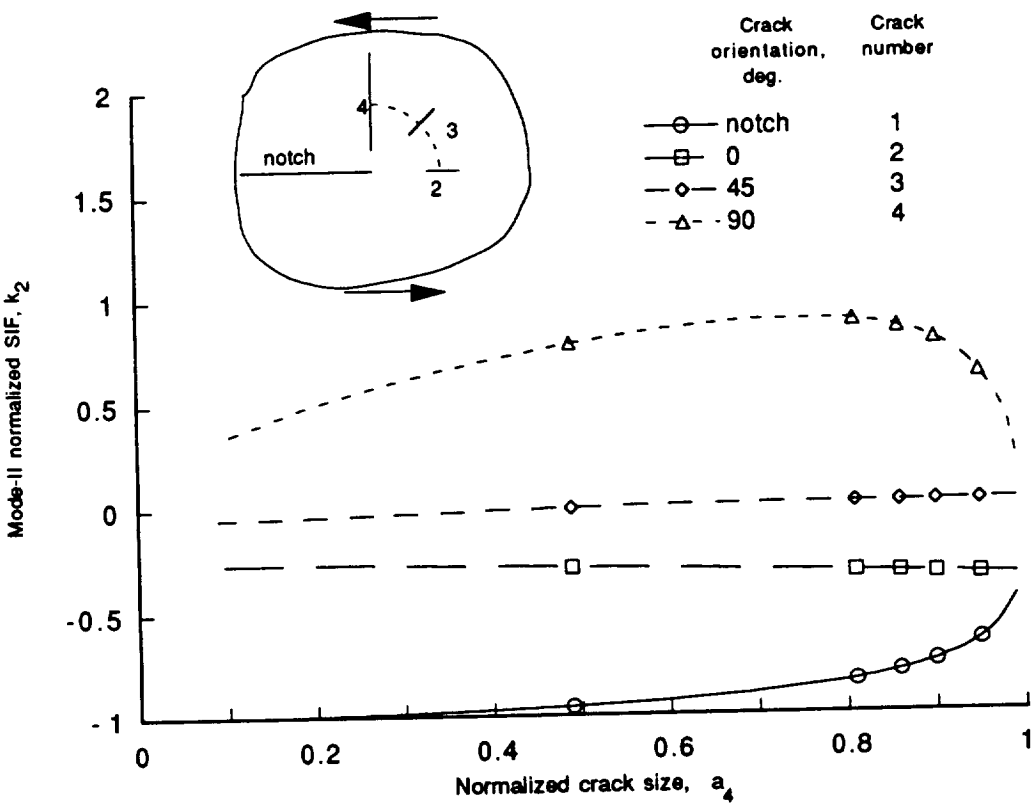

Fig. 13. Mode-II normalized SIF, k_2, for the inner crack tips versus the normalize crack size a_4 ($a_2 = a_3 = 0.1$, constant distance between the center of each crack to the origin of the global coordinate system, $|r_j| = 1$). Shear far field stress, σ_{XY}, load case.

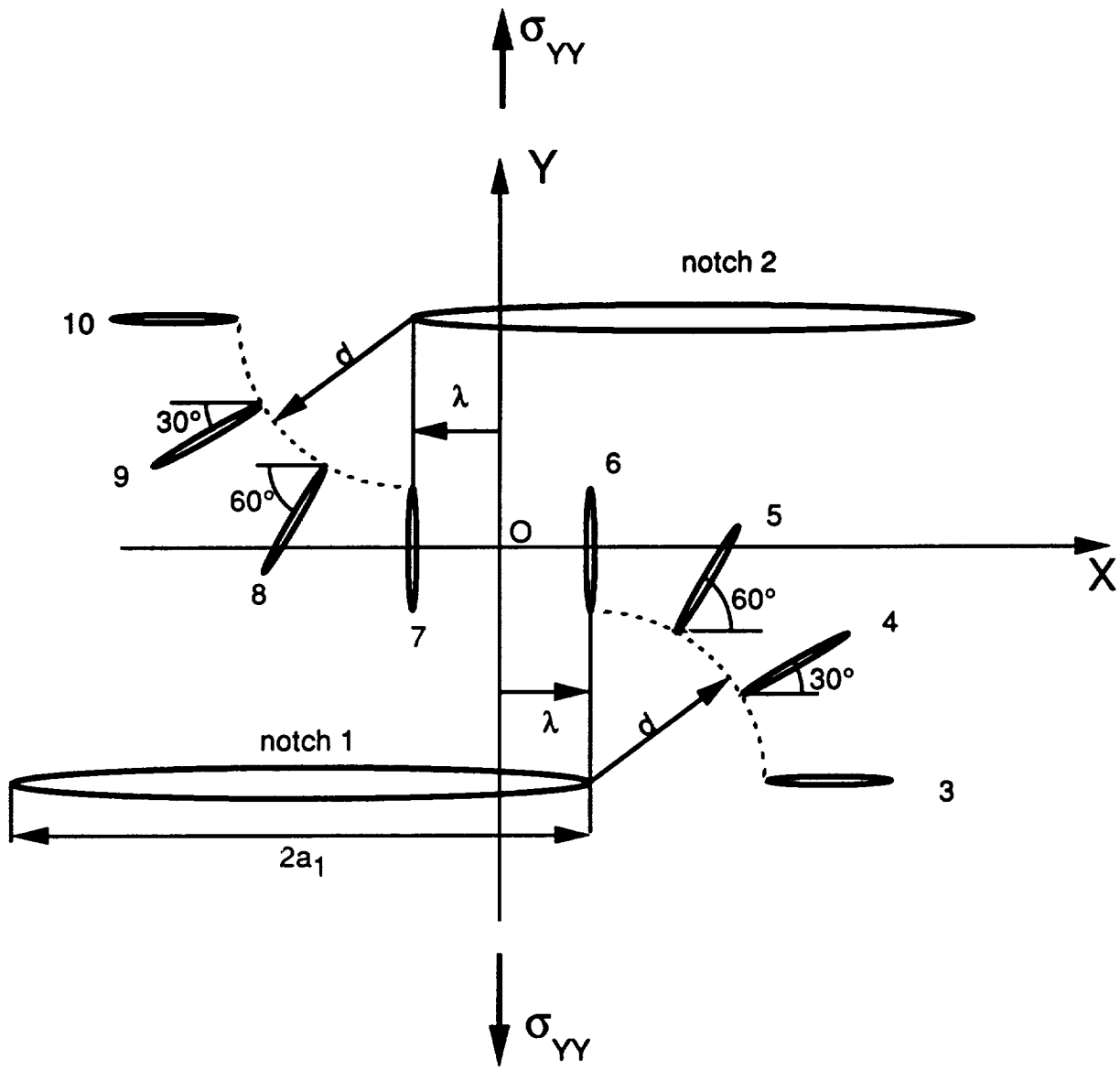

Fig. 14. Geometry describing the interacting two notches with eight microcracks.

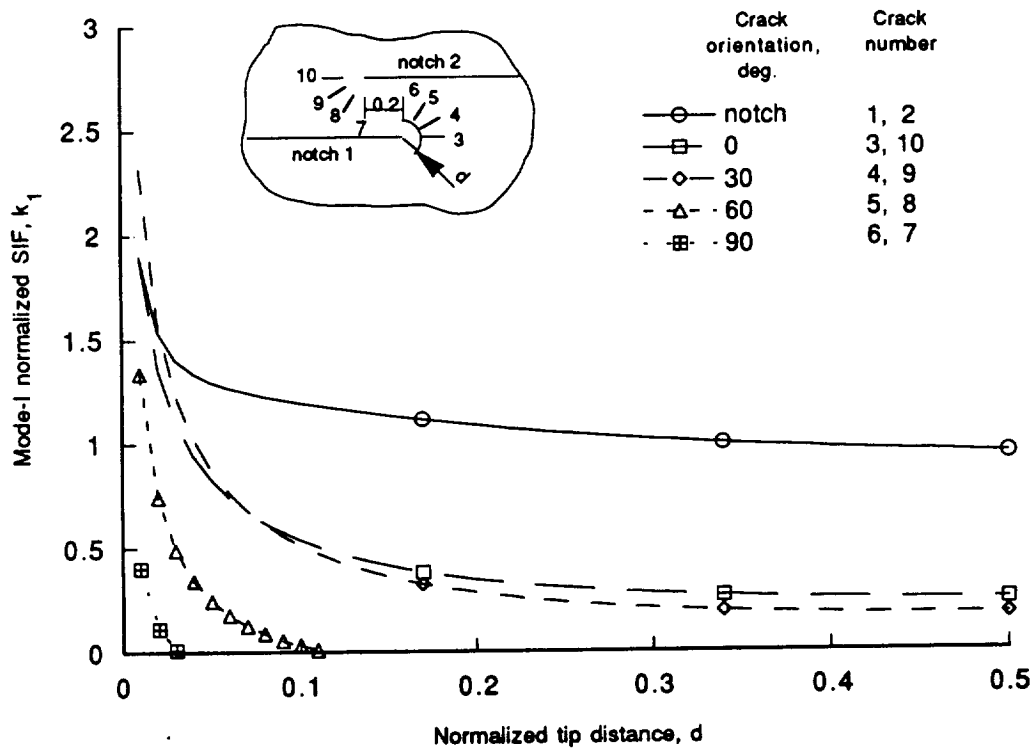

Fig. 15. Mode-I normalized SIF, k_1, for the inner crack tips versus normalized tip distance d ($a_1 = a_2 = 1$, $\lambda = 0.1$, $a_j = 0.1$ for j = 3,...,10).

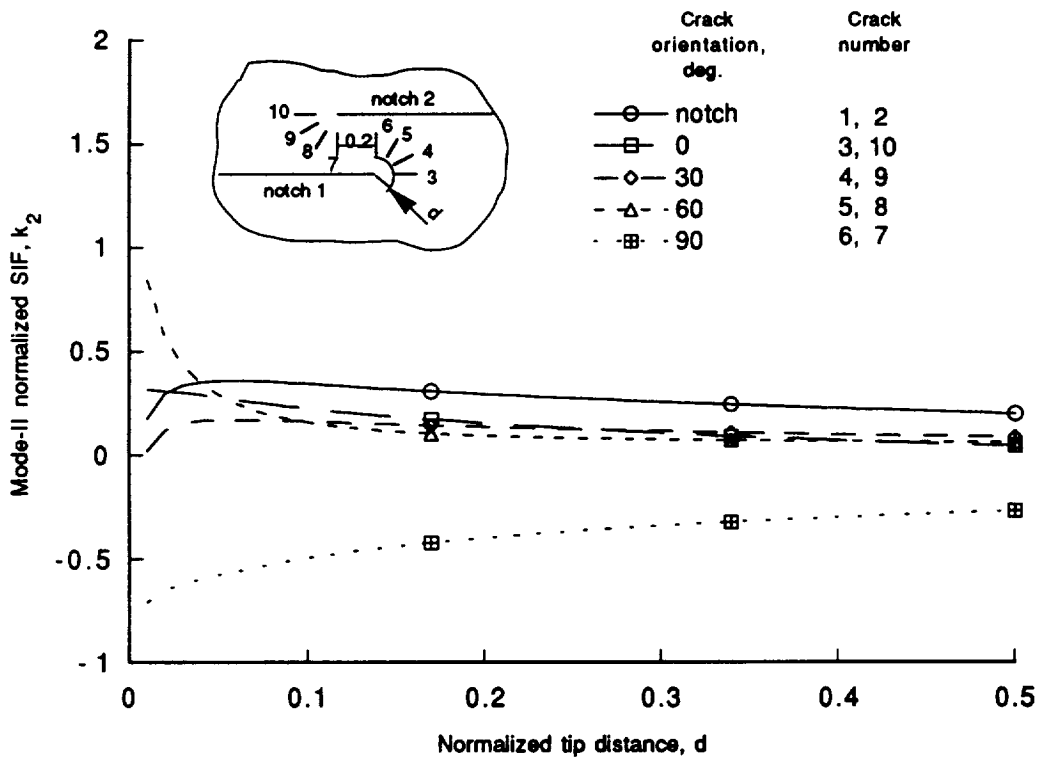

Fig. 16. Mode-II normalized SIF, k_2, for the inner crack tips versus normalized tip distance d ($a_1 = a_2 = 1$, $\lambda = 0.1$, $a_j = 0.1$ for j = 3,...,10).

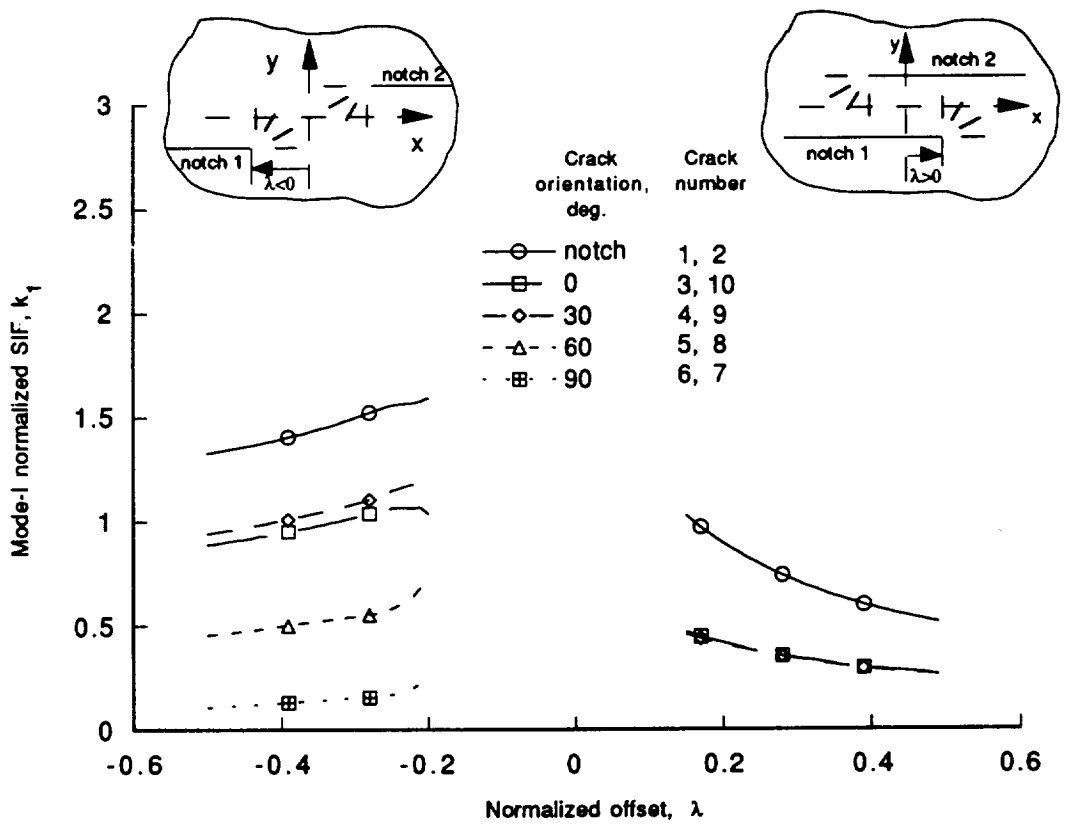

Fig. 17. Mode-I normalized SIF, k_1, for the inner crack tips versus normalized offset λ ($a_1 = a_2 = 1$, $d = 0.1$, $a_j = 0.1$ for j = 3,...,10).

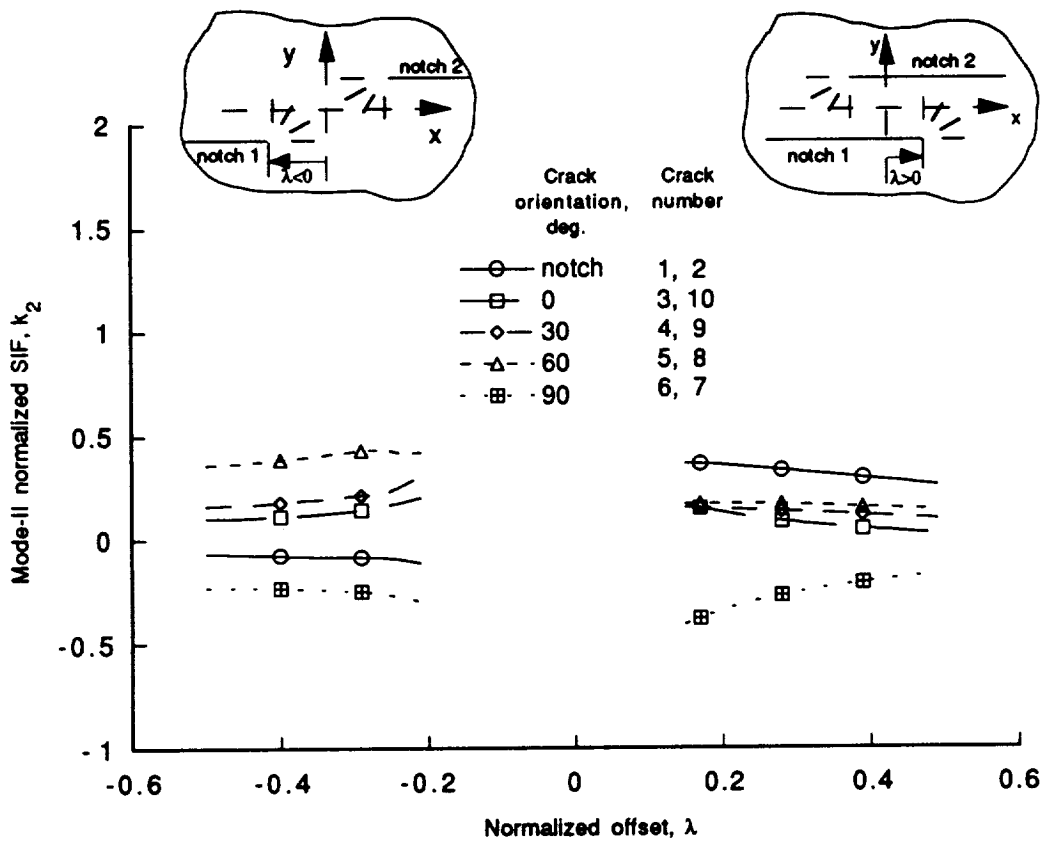

Fig. 18. Mode-II normalized SIF, k_2, for the inner crack tips versus normalized offset λ ($a_1 = a_2 = 1$, $d = 0.1$, $a_j = 0.1$ for j = 3,...,10).

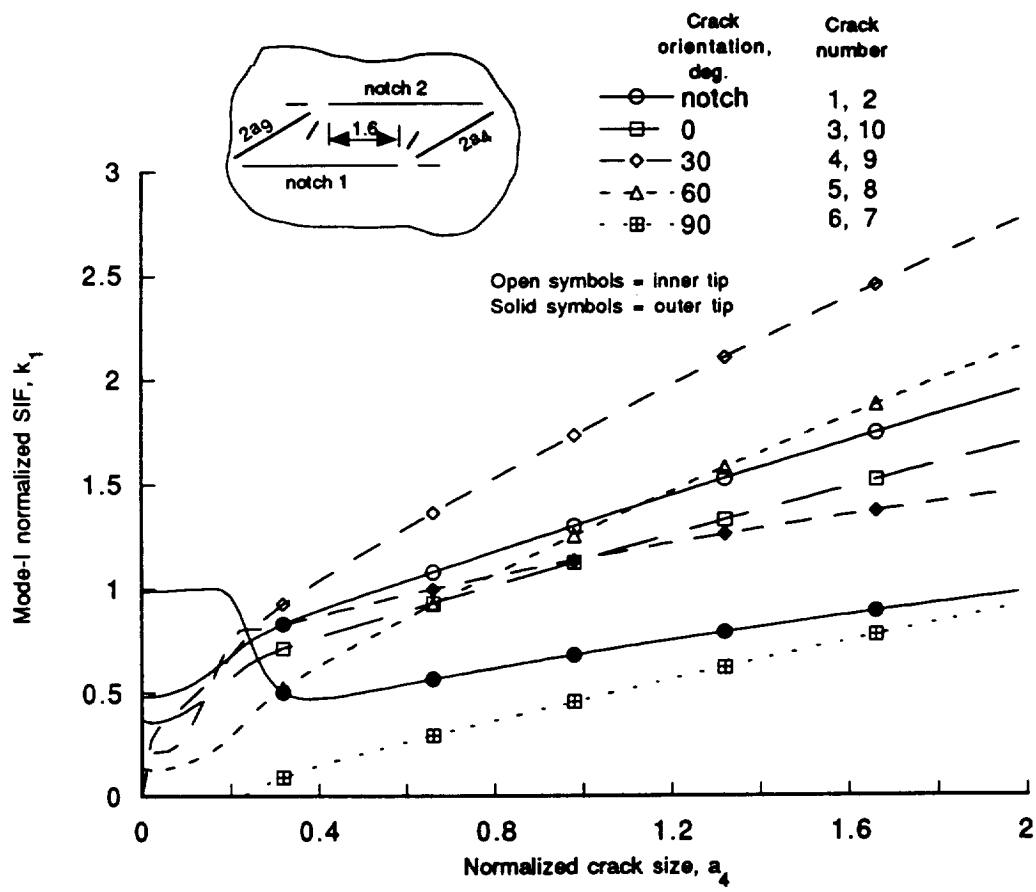

Fig. 19. Mode-I normalized SIF, k_1, for notches and cracks 4 and 9 tips and for the inner crack tips of cracks: 3, 5, 6, 7, 8, 10 ($a_1 = a_2 = 1$, $\lambda = 0.8$, $d = 0.1$, $a_3 = a_5 = a_6 = a_7 = a_8 = a_{10} = 0.1$).

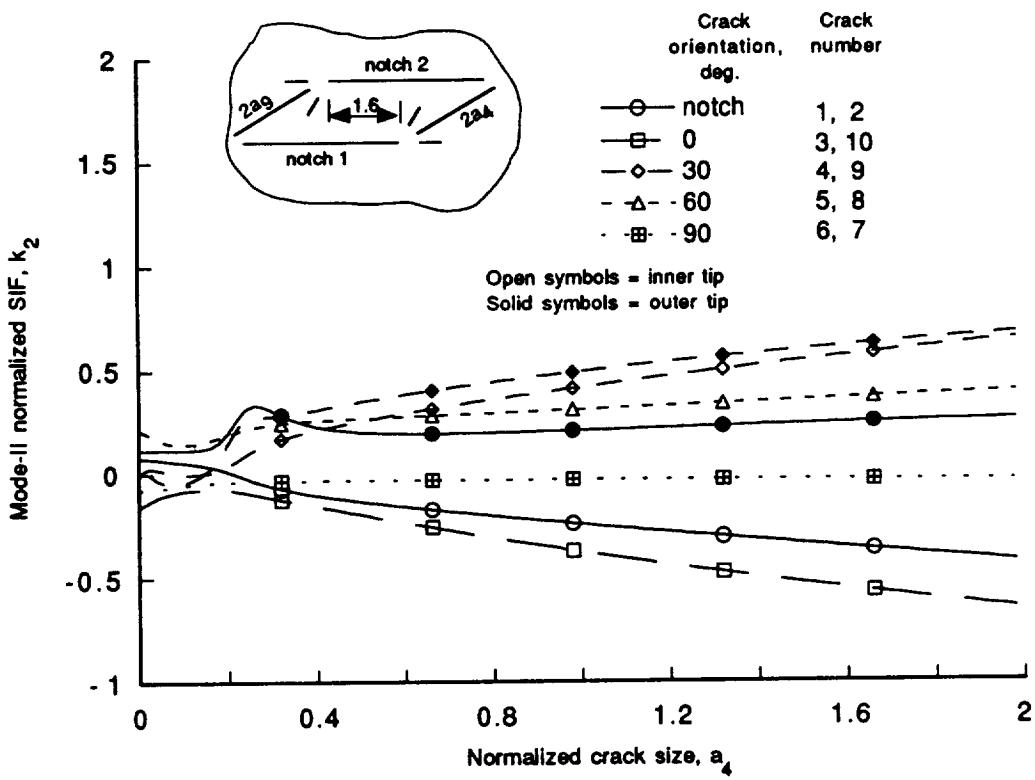

Fig. 20. Mode-II normalized SIF, k_2, for notches and cracks 4 and 9 tips and for the inner crack tips of cracks: 3, 5, 6, 7, 8, 10 ($a_1 = a_2 = 1$, $\lambda = 0.8$, $d = 0.1$, $a_3 = a_5 = a_6 = a_7 = a_8 = a_{10} = 0.1$).

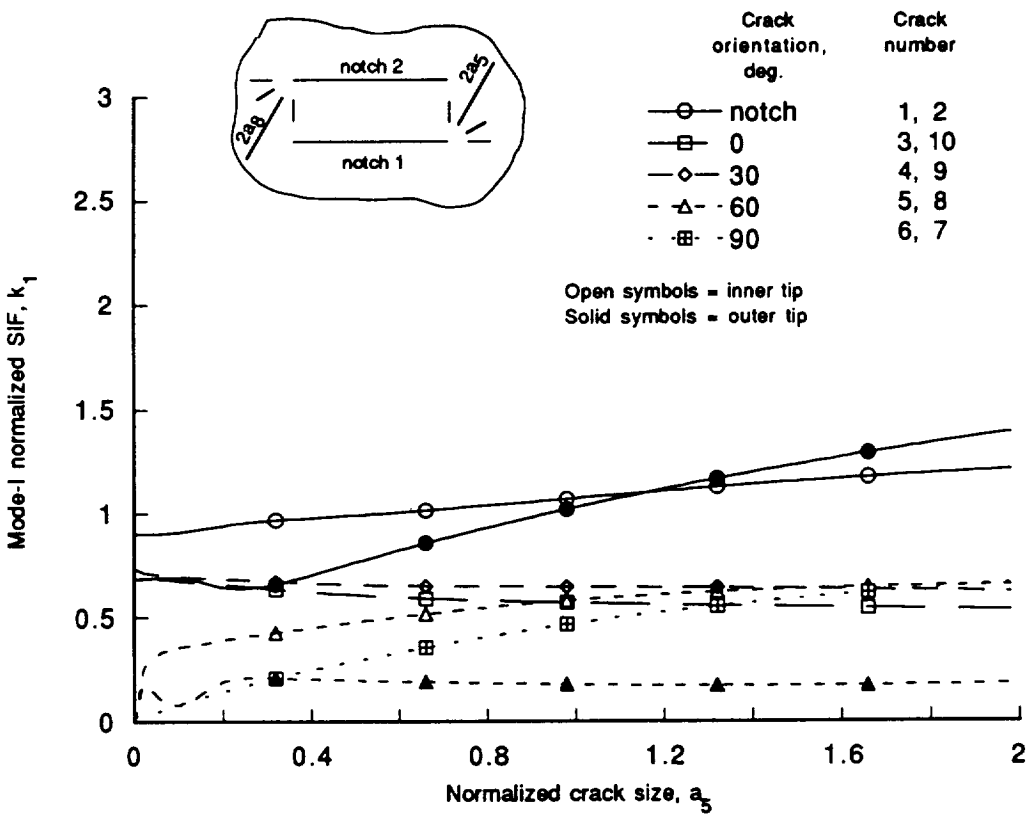

Fig. 21. Mode-I normalized SIF, k_1, for notches and cracks 4 and 9 tips and for the inner crack tips of cracks: 3, 4, 6, 7, 9, 10 ($a_1 = a_2 = 1$, $\lambda = 1.0$, $d = 0.1$, $a_3 = a_4 = a_6 = a_7 = a_9 = a_{10} = 0.1$).

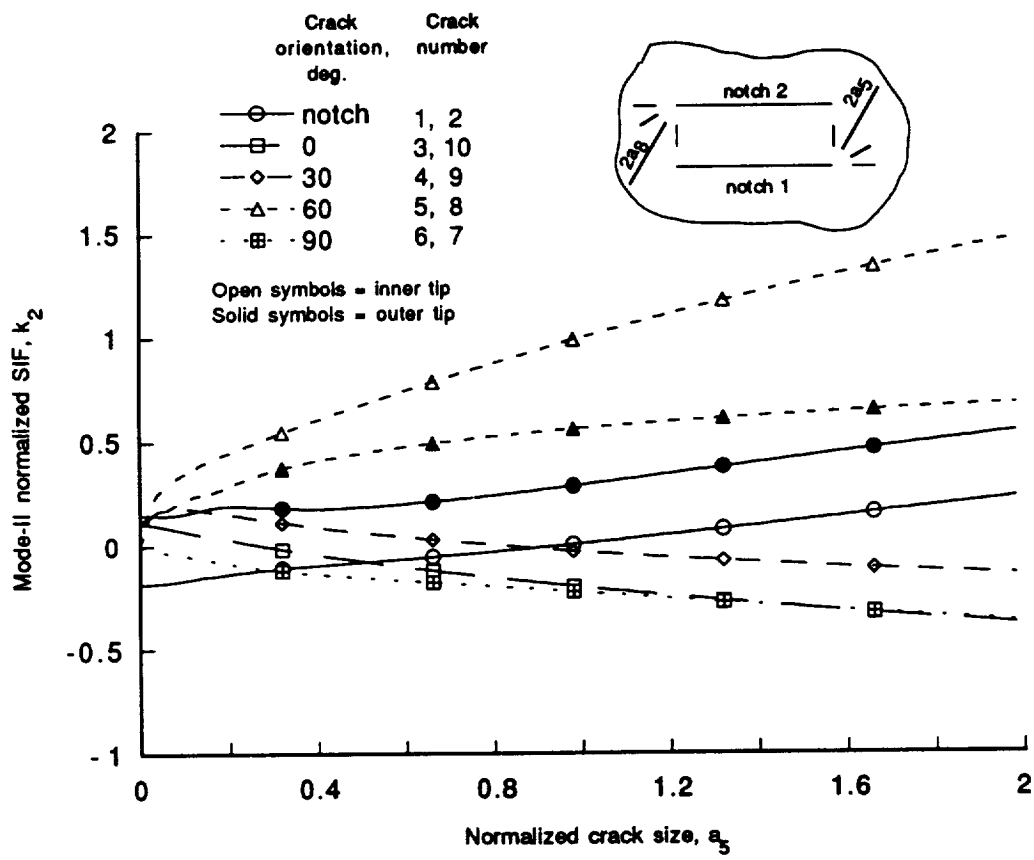

Fig. 22. Mode-II normalized SIF, k_2, for notches and cracks 4 and 9 tips and for the inner crack tips of cracks: 3, 4, 6, 7, 9, 10 ($a_1 = a_2 = 1$, $\lambda = 1.0$, $d = 0.1$, $a_3 = a_4 = a_6 = a_7 = a_9 = a_{10} = 0.1$).

REPORT DOCUMENTATION PAGE

Form Approved
OMB No. 0704-0188

Public reporting burden for this collection of information is estimated to average 1 hour per response, including the time for reviewing instructions, searching existing data sources, gathering and maintaining the data needed, and completing and reviewing the collection of information. Send comments regarding this burden estimate or any other aspect of this collection of information, including suggestions for reducing this burden, to Washington Headquarters Services, Directorate for Information Operations and Reports, 1215 Jefferson Davis Highway, Suite 1204, Arlington, VA 22202-4302, and to the Office of Management and Budget, Paperwork Reduction Project,(0704-0188), Washington, DC 20503.

1. AGENCY USE ONLY (*Leave blank*)

2. REPORT DATE
September 1992

3. REPORT TYPE AND DATES COVERED
Technical Memorandum

4. TITLE AND SUBTITLE
Calculation of Stress Intensity Factors in an Isotropic Multicracked Plate: Part II – Symbolic/Numeric Implementation

5. FUNDING NUMBERS
WU–510–01–50

6. AUTHOR(S)
S.M. Arnold, W.K. Binienda, H.Q. Tan, and M.H. Xu

7. PERFORMING ORGANIZATION NAME(S) AND ADDRESS(ES)
National Aeronautics and Space Administration
Lewis Research Center
Cleveland, Ohio 44135–3191

8. PERFORMING ORGANIZATION REPORT NUMBER
E–7254

9. SPONSORING/MONITORING AGENCY NAMES(S) AND ADDRESS(ES)
National Aeronautics and Space Administration
Washington, D.C. 20546–0001

10. SPONSORING/MONITORING AGENCY REPORT NUMBER
NASA TM–105823

11. SUPPLEMENTARY NOTES
S.M. Arnold, Lewis Research Center, Cleveland, Ohio, and W.K. Binienda, University of Akron, Department of Civil Engineering, Akron, Ohio 44325, and H.Q. Tan and M.H. Zu, University of Akron, Department of Mathematical Sciences, Akron, Ohio 44325. Responsible person, S.M. Arnold, (216) 433–3334.

12a. DISTRIBUTION/AVAILABILITY STATEMENT
Unclassified - Unlimited
Subject Category 39

12b. DISTRIBUTION CODE

13. ABSTRACT (*Maximum 200 words*)

Analytical derivations of stress intensity factors (SIF's) of a multicracked plate can be complex and tedious. Recent advances, however, in intelligent application of symbolic computation can overcome these difficulties and provide the means to rigorously and efficiently analyze this class of problems. Here, the symbolic algorithm required to implement the methodology described in Part I is presented. The special problem-oriented symbolic functions to derive the fundamental kernels are described, and the associated automatically generated FORTRAN subroutines are given. As a result, a symbolic/FORTRAN package named SYMFRAC, capable of providing accurate SIF's at each crack tip, has been developed and validated. Simple illustrative examples using SYMFRAC show the potential of the present approach for predicting the macrocrack propagation path due to existing microcracks in the vicinity of a macrocrack tip, when the influence of the microcracks' location, orientation, size and interaction are accounted for.

14. SUBJECT TERMS
Linear elastic fracture mechanics; Symbolic computation; Application

15. NUMBER OF PAGES
44

16. PRICE CODE
A03

17. SECURITY CLASSIFICATION OF REPORT
Unclassified

18. SECURITY CLASSIFICATION OF THIS PAGE
Unclassified

19. SECURITY CLASSIFICATION OF ABSTRACT
Unclassified

20. LIMITATION OF ABSTRACT